Bursts and Isolated Spikes Code for Opposite Movement Directions in Midbrain Electrosensory Neurons

Navid Khosravi-Hashemi[1,2], Maurice J. Chacron[1,2,3]*

1 Department of Physiology, McGill University, Montreal, Quebec, Canada, 2 Center for Applied Mathematics in Biology and Medicine, McGill University, Montreal, Quebec, Canada, 3 Department of Physics, McGill University, Montreal, Quebec, Canada

Abstract

Directional selectivity, in which neurons respond strongly to an object moving in a given direction but weakly or not at all to the same object moving in the opposite direction, is a crucial computation that is thought to provide a neural correlate of motion perception. However, directional selectivity has been traditionally quantified by using the full spike train, which does not take into account particular action potential patterns. We investigated how different action potential patterns, namely bursts (i.e. packets of action potentials followed by quiescence) and isolated spikes, contribute to movement direction coding in a mathematical model of midbrain electrosensory neurons. We found that bursts and isolated spikes could be selectively elicited when the same object moved in opposite directions. In particular, it was possible to find parameter values for which our model neuron did not display directional selectivity when the full spike train was considered but displayed strong directional selectivity when bursts or isolated spikes were instead considered. Further analysis of our model revealed that an intrinsic burst mechanism based on subthreshold T-type calcium channels was not required to observe parameter regimes for which bursts and isolated spikes code for opposite movement directions. However, this burst mechanism enhanced the range of parameter values for which such regimes were observed. Experimental recordings from midbrain neurons confirmed our modeling prediction that bursts and isolated spikes can indeed code for opposite movement directions. Finally, we quantified the performance of a plausible neural circuit and found that it could respond more or less selectively to isolated spikes for a wide range of parameter values when compared with an interspike interval threshold. Our results thus show for the first time that different action potential patterns can differentially encode movement and that traditional measures of directional selectivity need to be revised in such cases.

Competing Interests: The authors have declared that no competing interests exist.

* E-mail: maurice.chacron@mcgill.ca

Introduction

Motion perception is often required to control animal behavior such as tracking [1–5], postural balance [6–9] and prey capture [10,11]. Directional selectivity, in which neurons respond strongly to an object moving in a given direction ('preferred') but respond weakly or not at all when the same object moves in the opposite direction ('null'), is thought to provide a neural correlate of motion perception [12]. Directionally selective neurons have been found in several species including cats [12], rabbits [13], flies [14], and weakly electric fish [15–18].

Since the discovery of direction selective neurons [12], several models have been proposed to explain how this selectivity emerges in the brain [19–22]. Among these models, so called "Reichardt detectors" have received considerable attention and have been used to describe directional selectivity across several animal species [3,12–14,18,23–29]. These rely on two fundamental operations to generate directional selectivity [30,31]: first, asymmetric filtering of information from at least two separate zones within the receptive field generates a directional bias [13,14,18,27,32,33] and, second, subsequent nonlinear integration of these inputs [13,14,28,29,31,34,35].

Directional selectivity has been traditionally characterized by comparing the maximum firing rate obtained when a given object moves in a given direction to that obtained when the same object moves in the opposite direction. However, this does not take into account particular action potential patterns. Previous studies have shown that, for stationary stimuli, particular action potential patterns such as bursts (i.e. packets of action potential followed by quiescence) as well as isolated spikes could carry information that is qualitatively different than that carried by the full spike train [36–54]. However, whether these action potential patterns carry information about motion direction is poorly understood in general [26,43].

Weakly electric fish sense distortions of their self-generated electric organ discharge (EOD) via an array of electroreceptor neurons on their skin [55,56]. These electroreceptors synapse onto pyramidal cells within the hindbrain electrosensory lateral line lobe (ELL), which in turn project to the midbrain torus semicircularis (TS). It was previously shown that TS but not ELL neurons display directionally selective responses to moving objects [18,35]. The mechanism by which TS neurons generate directionally selective responses has been previously elucidated and is consistent with the Reichardt model. It consists of asymmetric filtering of afferent ELL input across the fish's body surface that is achieved by different time constants of synaptic depression across the receptive field [18] followed by nonlinear

integration of these inputs via subthreshold T-type calcium currents [26,35] (see [55] for review). We have recently found that bursts were more reliable indicators of motion direction than either the full spike or the isolated spike train in TS neurons [26]. These results suggest that isolated spikes actually code for other stimulus features than motion direction. However, a systematic analysis of movement direction coding by bursts and isolated spikes has not been carried out to date.

To address whether isolated spikes can actually code for motion direction, we systematically varied parameters in a previously established model of directional selectivity. Confirming our previous results, we found parameter regimes for which bursts were better indicators of motion direction than either the full spike or the isolated spike trains. However, we also found parameter regimes in which bursts and isolated spikes could both code for movement direction. Specifically, bursts were then preferentially elicited when the object moves in a given direction while isolated spikes were preferentially elicited when the object moves in the opposite direction. Further, our results show that, while the subthreshold T-type calcium conductance was not necessary to observe such regimes, it greatly enhanced the set of parameter values for which they were observed. Experimental recordings from TS neurons confirmed our model's prediction that bursts and isolated spikes can actually code for opposite movement directions. Finally, we considered a plausible neural circuit that can extract isolated spikes from a spike train and quantified this circuit's ability to extract the isolated spikes from a spike train consisting of a mixture of bursts and isolated spikes. Our results show for the first time that different action potential patterns in a given neuron can carry information about different movement directions and suggest that differential coding of stimulus attributes by bursts and isolated spikes is a general feature of sensory processing that is applicable to a wide range of stimuli including motion.

Results

Bursts and isolated spikes can code for opposite movement directions

Our biophysical model is based on the Hodgkin-Huxley formalism [57] (see Materials and Methods). The receptive field is modeled in one dimension as two adjacent zones (ON and OFF) that have time constants of depression τ_{ON} and τ_{OFF}, respectively (Fig. 1A). In this model, the OFF zone represents the output of I-type (i.e. inhibited by increases in the stimulus) ELL pyramidal cells and the ON zone represents the output of E-type (i.e. excited by increases in the stimulus) ELL pyramidal cells as both cell types made excitatory connections onto TS neurons [58]. The summed input from each zone is convolved with an alpha function to mimic the synaptic PSP shape and fed into a Hodgkin-Huxley model with leak, spiking sodium, delayed rectifier potassium, and T-type calcium conductances (Fig. 1A, see Materials and Methods). T-type calcium channels are inactivated at resting membrane potential values (i.e. ~ -60 mV) and require ~ 100 ms hyperpolarisation to ~ -70 mV in order to remove their inactivation after which a subsequent depolarisation will lead to a subthreshold calcium spike, leading to nonlinear integration of synaptic input. Moreover, bursts of sodium action potentials can occur on top of these calcium spikes [59,60]. However, a simple depolarization from the resting potential will not lead to burst firing as the calcium channel is still inactivated and will instead lead to isolated spike firing [60]. We mimicked the effect of the massive synaptic bombardment that neurons receive under in vivo conditions [61], by including a noise term that causes membrane potential fluctuations. This noise term can give rise to a mixture of

burst and isolated action potential firing as observed for TS neurons under in vivo conditions [26].

The stimulus consists of an object that moves across the receptive field in both directions (see Materials and Methods). Fig. 1B shows the outputs from the ON and OFF zones to this stimulus. When the object moves from left to right (i.e. from the OFF zone to the ON zone), the hyperpolarisation from the OFF zone precedes the depolarization from the ON zone. However, when the object moves in the opposite direction (i.e. from the ON zone to the OFF zone), the depolarisation from the ON zone is truncated by the hyperpolarisation from the OFF zone (Fig. 1C). The membrane potential responses of the model neuron to these moving stimuli are shown in Fig. 1D. When the object moves from left to right, the hyperpolarisation from the OFF zone removes the inactivation of the calcium conductance and the depolarisation from the ON zone activates this conductance, which tends to result in a burst of action potentials (Fig. 1D, top). In contrast, when the object moves in the opposite direction, the depolarisation from ON zone is not preceded by a hyperpolarisation, and thus tends to elicit isolated action potentials (Fig. 1D, top).

We used an ISI threshold criterion to separate the model's output spiketrain into bursts and isolated spikes (Fig. 1D, bottom, see Materials and Methods). Specifically, when a given interspike interval was less than the threshold, the two spikes associated with this interspike interval were considered to belong to a burst [41,42,44]. The spikes that were not deemed part of a burst were labelled isolated spikes (Fig. 1D, bottom). We used this criterion to separate the spike train into the burst train (i.e. the train of action potentials that belong to bursts) and the isolated spike train (i.e. the train of action potentials that do not belong to bursts) (see Materials and Methods).

The response of our model to this stimulus is presented in Fig. 2. When we used the full spike train to compute the peri-stimulus time histogram (PSTH), the model displayed a strong response when the object moved in the left to right direction and a weaker response when the object moved in the right to left direction (Figs. 2A and 2B, middle). We quantified this difference using a directional bias (DB) index that ranges between -1 and 1 with 0 implying no directional selectivity (see Materials and Methods). Specifically, DB values of 1 and -1 indicate complete direction preference for movement from left to right and from right to left, respectively, while a value of 0 indicates no direction selectivity. We found that this neuron displayed selectivity to the object moving from left to right when using the full spike train (DB = 0.51) (Fig. 2C purple column).

However, qualitatively different results were obtained when we instead used the burst and isolated spike trains to compute the PSTH from this same neuron. We found that bursts mostly occurred when the object moved from left to right (Fig. 2A arrows; Fig. 2C green column), thereby giving rise to a larger directional bias (DB = 0.72) than that of the full spike train. In contrast, isolated spikes mostly occurred when the object moved from right to left (Fig. 2A arrows; Fig. 2C orange column), giving rise to a negative directional bias (DB = -0.34). These results show that bursts and isolated spikes can encode opposite directions of movement.

Effects of T-type calcium channels on movement direction coding by bursts and isolated spikes

We next investigated movement direction coding by bursts and isolated spikes in our model without the calcium conductance. To do this, we performed numerical simulations of our model with $g_T = 0$. We note that our model then does not generate calcium-mediated burst firing, but can generate short interspike intervals
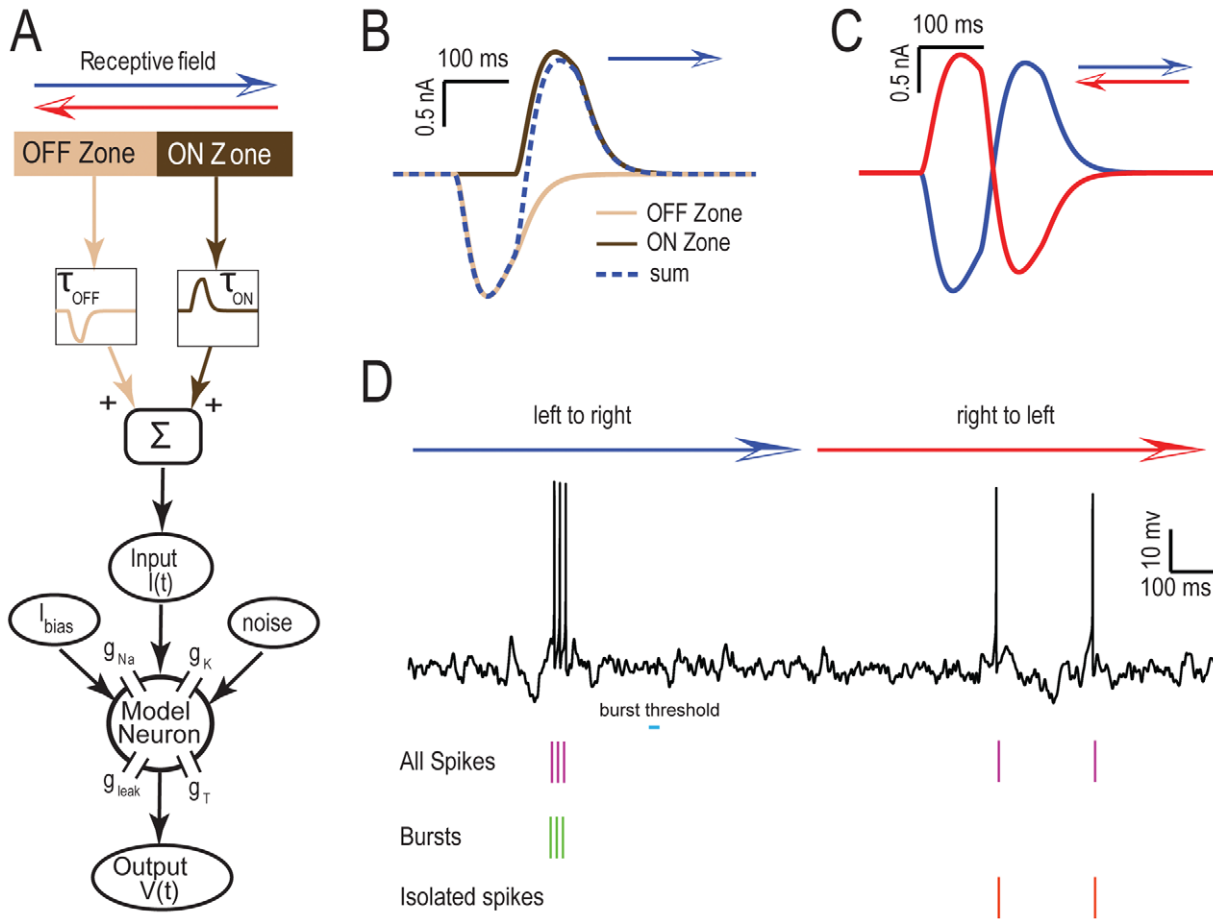
Figure 1. Modeling directional selectivity in TS neurons. A) Schematic of our model. The receptive field is composed of two zones: the OFF zone which represents the output of I-type ELL pyramidal cells with synaptic depression time constant τ_{OFF} while the ON zone represents the output of E-type ELL pyramidal cells with synaptic depression time constant τ_{ON}. The responses from each zone are then fed into a Hodgkin-Huxley model with spiking sodium (g_{Na}), delayed rectifier potassium (g_K), leak (g_{leak}), and T-type calcium (g_T) conductances. Noise is also added to this model in order to mimic synaptic input from other neurons. **B**) Inputs from OFF zone (beige), ON zone (brown), and the sum of the two (dashed blue) for $\tau_1 = \tau_2 = 500$ msec when the object moves from left to right (i.e. from the OFF zone to the ON zone). **C**) Summed input from both zones when the object moves from left to right (blue) and from right to left (red). **D**) Segregating the spike train to bursts and isolated spikes. The top trace is an example membrane potential trace for one trial (object moves from left to right and then from right to left) from our model in response to the inputs shown in C. Spikes (purple lines) belonging to interspike intervals that were less than the burst threshold (cyan) were identified as belonging to bursts (green lines) while those that do not were identified as isolated spikes (red lines).
doi:10.1371/journal.pone.0040339.g001

that would be considered as "bursts" according to the ISI threshold criterion when the bias current is sufficiently high. We found that our model displayed a stronger response when the object moved from right to left and a weaker response when the object moved from left to right when the full spike train was used (Fig. 3A, Fig. 3B middle). Our model thus still displayed directional selectivity (DB = −0.46). When we used the burst train, we observed a stronger directional bias (DB = −0.97) as bursts were almost exclusively elicited when the object moves from right to left. In contrast, the isolated spikes tended to be elicited when the object moves in both directions with a slight bias when the object moves from right to left as reflected by a weaker directional bias (DB = −0.21). As such, our results show that both bursts and isolated spikes encoded the same movement direction (i.e. right to left) when we set $g_T = 0$ in our model as they displayed negative directional biases (Fig. 3C).

In order to better understand these results, we then plotted the inputs to the model when the object moves from left to right

(Fig. 4A, left) and right to left (Fig. 4A. right). In the left to right direction, the hyperpolarisation from the OFF zone attenuates the subsequent depolarisation from the ON zone (Fig. 4A, left). In contrast, in the right to left direction, the initial depolarisation from the ON zone is truncated by the subsequent hyperpolarisation from the OFF zone (Fig. 4A, right). The response of our model to these different inputs strongly depends on the value of the T-type conductance g_T. When g_T is present, the initial hyperpolarisation from the OFF zone removes the inactivation of this conductance and the subsequent depolarization activates it, thereby causing a burst of action potentials as explained above when the object moves from left to right (Fig. 4B, left). In contrast, the initial depolarisation gives rise to isolated spikes when the object moves from right to left as the T-type conductance is then inactivated (Fig. 4B, right). The following hyperpolarisation only partially removes this inactivation and the subsequent repolarization gives rise to a burst of action potentials albeit with a larger intraburst interval (Fig. 4B, right). Therefore, our model tends to
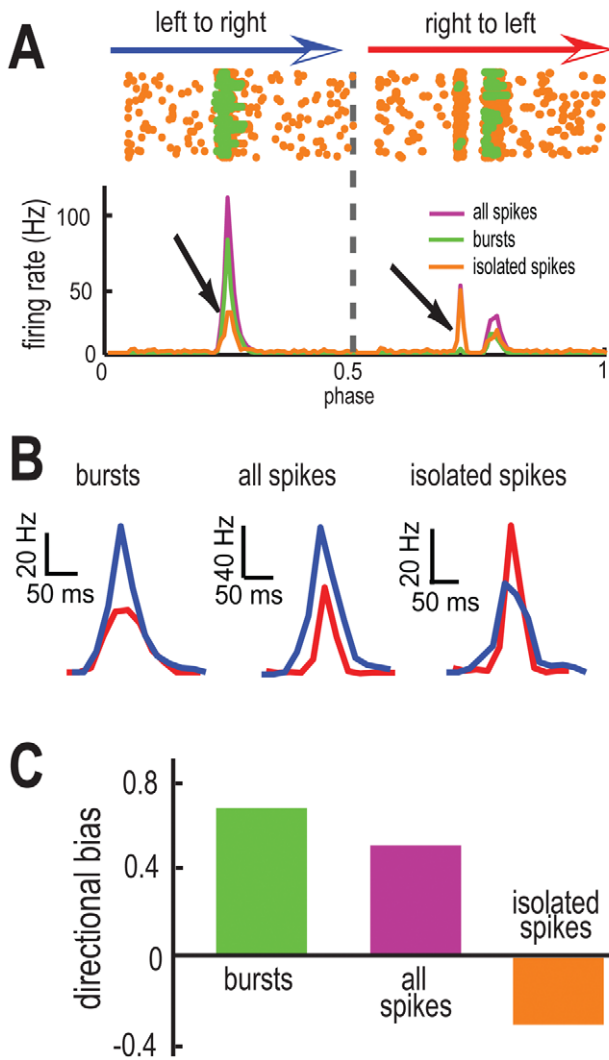
Figure 2. Bursts and isolated spikes code for opposite movement directions. A) Raster plot (top) obtained for $\tau_{ON} = 5$ msec, $\tau_{OFF} = 500$ msec from our model. Each dot represents the time at which an action potential occurs. These are color coded as orange for isolated spikes and green for burst spikes. PSTH (bottom) obtained from all spikes (purple), burst spikes (green), and isolated spikes (orange). **B)** PSTH values near the maximum values in the left to right (blue) and right to left (red) directions for burst spikes (left), all spikes (middle), and isolated spikes (right). Note the opposite directional preference of isolated spikes (brown arrow). **C)** Directional biases computed from burst spikes (green), all spikes (purple), and isolated spikes (orange).
doi:10.1371/journal.pone.0040339.g002

Figure 3. T-type calcium channels promote coding of opposite movement directions by bursts and isolated spikes. A) Raster plot (top) obtained for $\tau_{ON} = 5$ msec, $\tau_{OFF} = 500$ msec when $g_T = 0$. The spikes in the raster plot are color coded, as orange for isolated spikes and green for burst spikes. PSTH curves (bottom) obtained from all spikes (purple), burst spikes (green), and isolated spikes (orange). **B)** PSTH values near the maximum values in the left to right (blue) and right to left (red) directions for burst spikes (left), all spikes (center), and isolated spikes (right). **C)** Directional biases computed from all spikes (green), burst spikes (purple), and isolated spikes (orange). We note that the error bars are too small to be shown.
doi:10.1371/journal.pone.0040339.g003

respond with a mixture of bursts and isolated spikes when the object moves from right to left.

Qualitatively different results were seen when we removed the T-type conductance (i.e. $g_T = 0$). When the object moves from left to right, the depolarization from the ON zone is partially occluded by the preceding hyperpolarisation from the OFF zone and thus gives rise to isolated spiking (Fig. 4C, left). When the object moves from right to left, the initial depolarisation from the ON zone gives rise to a burst of action potentials. The subsequent hyperpolarization from the OFF zone silences spiking and the repolarisation then gives rise to isolated spikes (Fig. 4C, right). As such, our model gives rise to isolated spikes when the object moves in both directions and to bursts preferentially when the object moves from right to left.
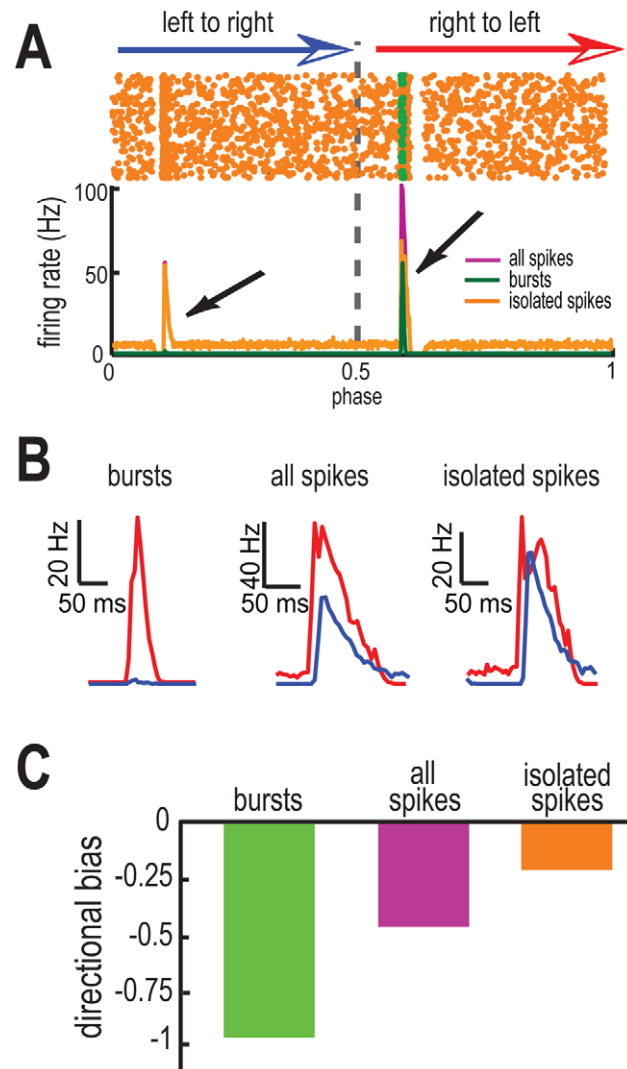
Exploring the effect of the synaptic depression time constants on movement direction coding by bursts and isolated spikes

We then systematically varied model parameters and characterized the directional biases of bursts and isolated spikes with the T-type conductance present. We first varied the synaptic depression time constants from the ON (τ_{ON}) and OFF (τ_{OFF}) zones in our model. Our results show that varying these can lead to dramatic qualitative differences between the directional biases of bursts and isolated spikes. Indeed, for small τ_{OFF} and large τ_{ON} values (i.e. τ_{OFF} <0.1 sec and τ_{ON} >0.1 sec), the full (Fig. 5A), burst (Fig. 5B), and isolated (Fig. 5C) spike trains all displayed positive directional biases and thus encoded the same movement direction. However, the
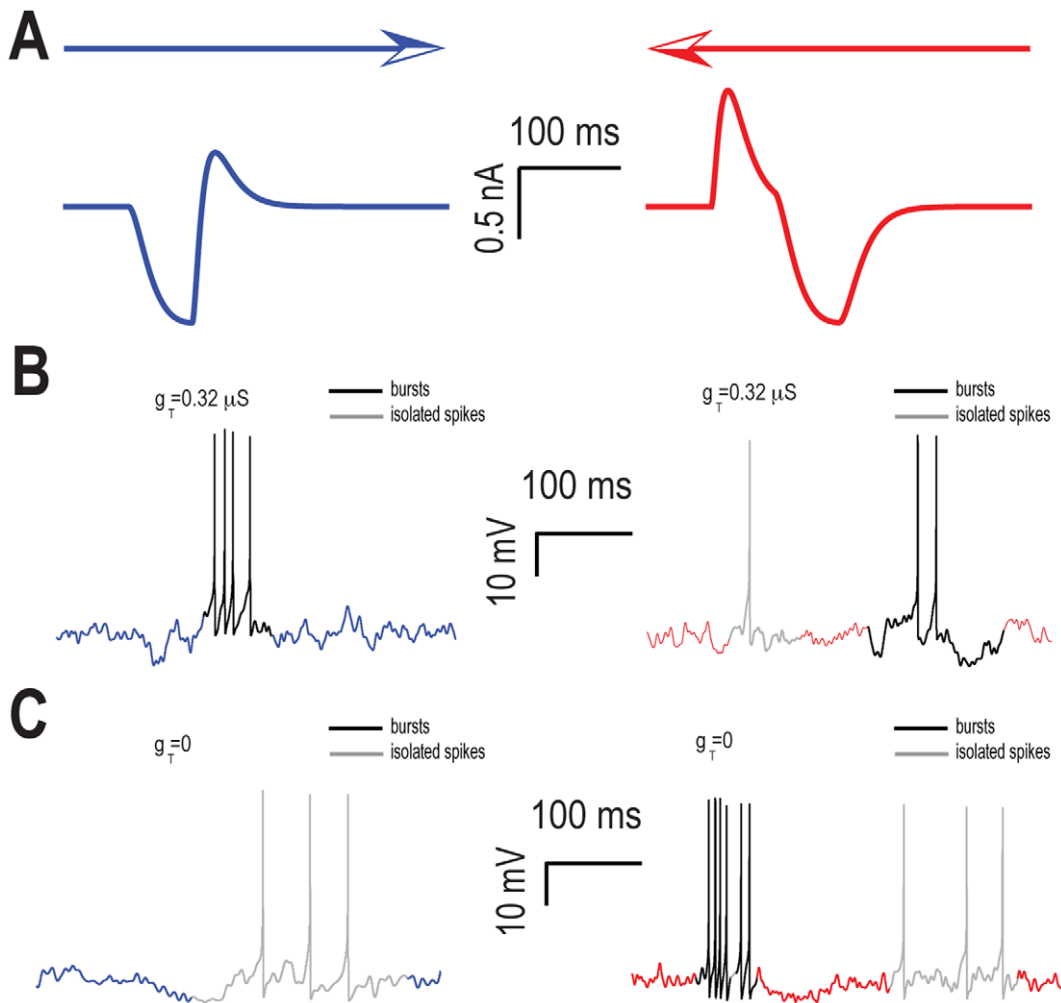
Figure 4. T-type calcium channels promote burst and isolated spike firing when the object moves in opposite directions. A) Summed input currents from both zones when the object moves from left to right (blue) and from right to left (red) for $\tau_{ON} = 5$ msec, $\tau_{OFF} = 500$ msec. **B**) Example membrane potential traces when the object moves from left to right (left) and from right to left (right) with the T-type calcium conductance. The response consisted of bursts (black) when the object moved from left to right and of bursts (black) and isolated spikes (gray) when the object moved from right to left. **C**) Example membrane potential traces when the object moves from left to right (blue) and from right to left (red) without the calcium conductance. The response consisted of isolated spikes (gray) when the object moved from left to right and of bursts (black) and isolated spikes (gray) when the object moved from right to left.
doi:10.1371/journal.pone.0040339.g004

directional bias of isolated spikes was smaller in magnitude than that of the full and burst trains, which corresponds to the regime described in our previous study [26]. We will henceforth refer to this regime as "same direction selectivity". In contrast, for large τ_{OFF} and small τ_{ON} values (i.e. $\tau_{OFF} > 0.1$ sec and $\tau_{ON} < 0.1$ sec), both the full (Fig. 5A) and burst (Fig. 5B) trains displayed a positive directional bias while the isolated spike train (Fig. 5C) displayed a negative directional bias. We will henceforth refer to this regime as "opposite direction selectivity".

In order to better characterize both regimes, we computed an opposite directionality index (ODI, see Materials and Methods). This index is positive when the directional biases of both bursts and isolated spikes have the same sign, negative when they are opposite in sign, and 0 when one does not display significant directional selectivity. We found that the ODI was positive for small τ_{OFF} and large τ_{ON} values (i.e. $\tau_{OFF} < 0.1$ sec and $\tau_{ON} > 0.1$ sec) and negative for large τ_{OFF} and small τ_{ON} values (i.e. $\tau_{OFF} > 0.1$ sec and $\tau_{ON} < 0.1$ sec) (Fig. 5D).

In order to better understand why varying the depression time constants τ_{ON} and τ_{OFF} can give rise to qualitatively different

regimes, we plotted the PSTH curves for the full, burst, and isolated spike trains for two sets of parameter values that gave rise to same and opposite direction selectivity regimes in Figs. 5E and 5F, respectively. The parameter values used for the same and opposite direction selectivity regimes are shown in Fig. 5D as points "E" and "F", respectively. For the same direction selectivity regime, the maximum firing rate from the full, burst, and isolated spike trains was strongest when the object moves from left to right (Fig. 5E). In contrast, for the opposite directional selectivity regime, the maximum firing rate for the full spike and burst trains were higher when the object moves from left to right while that of isolated spike train is highest when the object moves from right to left (Fig. 5F).

We thus conclude that the ratio τ_{OFF}/τ_{ON} has a strong influence on whether bursts and isolated spikes code for the same or opposite movement directions. Indeed, the former regime tended to occur for low values of τ_{OFF}/τ_{ON} while the latter regime tended to occur for high values of τ_{OFF}/τ_{ON}. We also varied the gains from the ON and OFF zones, G_{ON} and G_{OFF}, and found that varying these gave rise
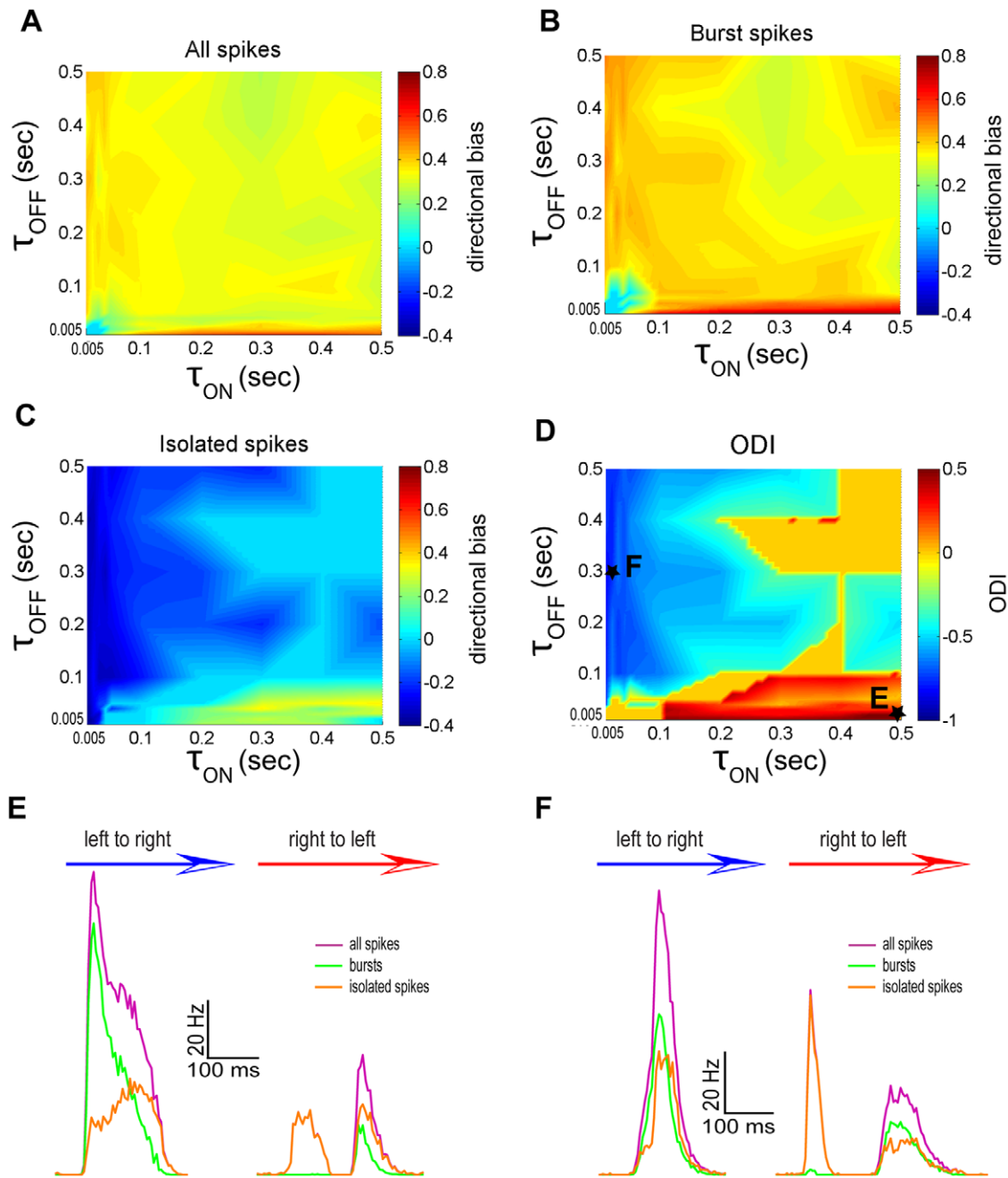
Figure 5. The synaptic depression time constants τ_{ON} and τ_{OFF} strongly influence movement direction coding by bursts and isolated spikes. A) Directional bias computed from the full spike train as a function of τ_{ON} and τ_{OFF}. **B)** Directional bias computed from the burst spike train as a function of τ_{ON} and τ_{OFF}. **C)** Directional bias computed from the isolated spike train as a function of τ_{ON} and τ_{OFF}. **D)** Opposite direction selectivity index (ODI) as a function of τ_{ON} and τ_{OFF}. **E)** PSTH values near the maximum values in the left to right (blue arrow) and right to left (red arrow) directions for the full spike (purple), burst (green), and isolated (orange) spike trains for an example data point marked with a star in panel D. **F)** PSTH values near the maximum values in the left to right (blue arrow) and right to left (red arrow) directions for the full spike (purple), burst (green), and isolated (orange) spike trains for another example data point marked with a star in panel D.
doi:10.1371/journal.pone.0040339.g005

to qualitatively similar results in that opposite movement direction regimes were mostly seen for high values of G_{OFF}/G_{ON} (Fig. S1).

Exploring the effect of bias current on movement direction coding by bursts and isolated spikes

We next explored whether the bias current I_{bias} influenced coding of movement direction by bursts and isolated spikes. To do so, we plotted the directional biases of the full (Fig. 6A), burst

(Fig. 6B), and isolated (Fig. 6C) spike trains as a function of both the bias current I_{bias} and the ratio of the synaptic depression time constants τ_{OFF}/τ_{ON} which was varied so as to observe both same and opposite direction selectivity regimes (see Materials and Methods). Our results show that when I_{bias} was low (i.e. < -1.8 nA) or high (i.e. > -0.5 nA), neither bursts (Fig. 6B) nor isolated spikes (Fig. 6C) displayed significant directional selectivity, resulting in an ODI of zero (Fig. 6D). Regimes in which the
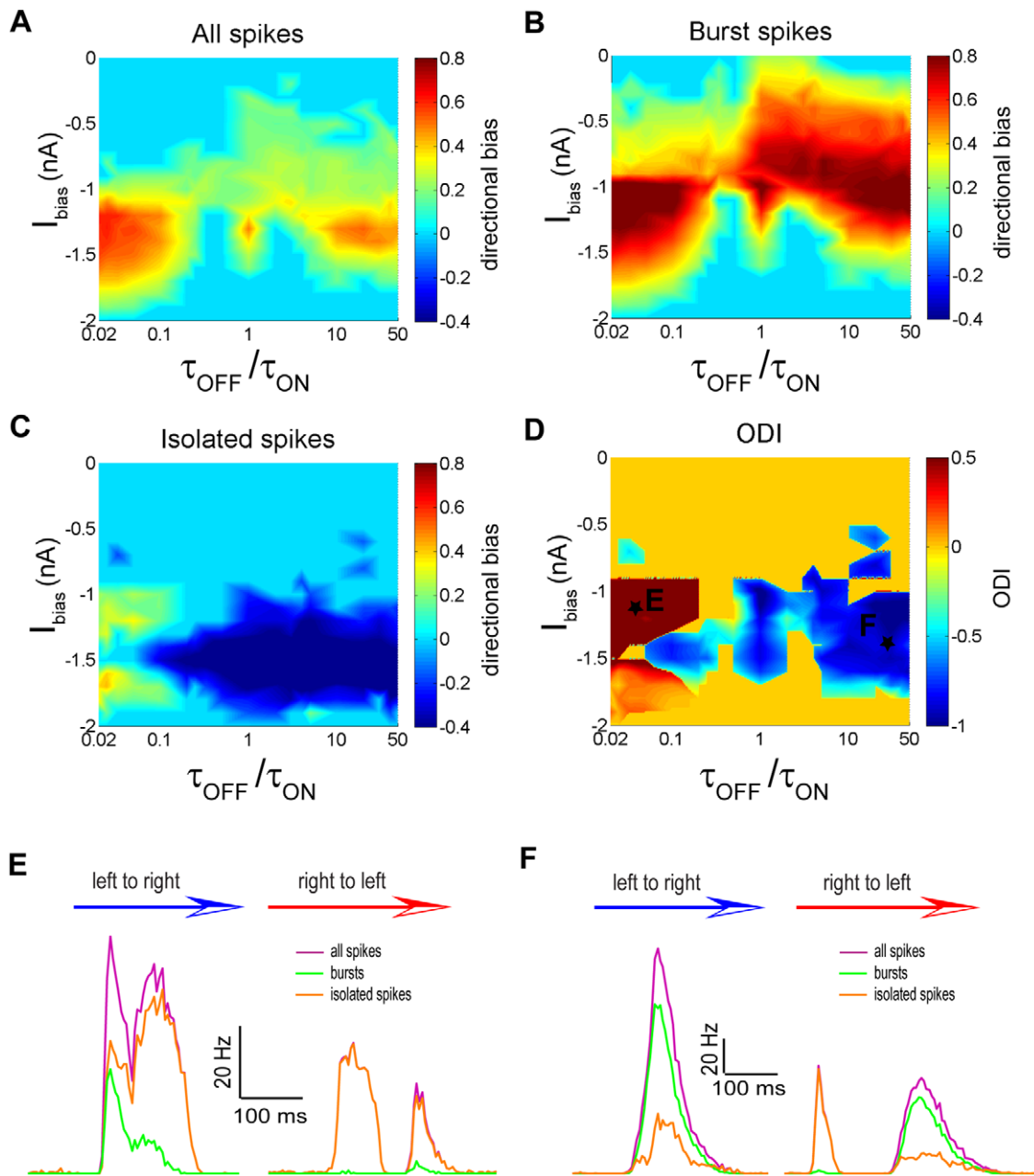
Figure 6. The bias current I_bias and synaptic depression time constant ratio τ_{OFF}/τ_{ON} strongly influence movement direction coding by bursts and isolated spikes. A) Directional bias computed from the full spike train as a function of τ_{OFF}/τ_{ON} and I_{bias}. **B)** Directional bias computed from the burst train as a function of τ_{OFF}/τ_{ON} and I_{bias}. **C)** Directional bias computed from the isolated spike train as a function of τ_{OFF}/τ_{ON} and I_{bias}. **D)** Opposite direction selectivity index as a function of τ_{OFF}/τ_{ON} and I_{bias}. **E)** PSTH values near the maximum values in the left to right (blue arrow) and right to left (red arrow) directions for the full spike (purple), burst (green), and isolated (orange) spike trains for an example data point marked with a star in panel D. **F)** PSTH values near the maximum values in the left to right (blue arrow) and right to left (red arrow) directions for the full spike (purple), burst (green), and isolated (orange) spike trains for another example data point marked with a star in panel D.
doi:10.1371/journal.pone.0040339.g006

ODI was non-zero tended to occur for intermediate values of I_{bias} (i.e. -1.8 nA$<I_{bias}<-0.5$ nA). For low values of τ_{OFF}/τ_{ON} (i.e. $\tau_{OFF}/\tau_{ON}<0.2$), we observed same directional selectivity regimes characterized by positive ODI (Fig. 6D). In contrast, for high values of τ_{OFF}/τ_{ON} (i.e. $\tau_{OFF}/\tau_{ON}>0.2$), we observed regimes of opposite direction selectivity characterized by negative ODI (Fig. 6D). In particular, we found that, for some parameter values (i.e. $I_{bias}=-1$ nA and $\tau_{OFF}/\tau_{ON}=1$), the full spike train displayed weak directional selectivity (Fig. 6A) while both the burst (Fig. 6B)

and isolated (Fig. 6C) spike trains displayed strong selectivity for opposite movement directions. We return to this point below in the discussion.

The PSTH curves for the full, burst, and isolated spike trains are shown for two sets of parameter values that gave rise to same and opposite direction selectivity regimes in Figs. 6E and 6F, respectively. The parameter values used for the same and opposite direction selectivity regimes are shown in Fig. 6D as points "E" and "F", respectively. For the same direction selectivity regime,

the maximum firing rate from the full spike, burst, and isolated spike trains was strongest when the object moves from left to right (Fig. 6E). On the other hand, for the opposite directional selectivity regime, the maximum firing rates for the full spike and the burst trains were both greatest when the object moves from left to right while that of isolated spikes was greatest when the object moves from right to left (Fig. 6F).

T-type calcium currents promote coding of opposite movement directions by bursts and isolated spikes

We next explored how different parameters influenced movement coding by bursts and isolated spikes in our model without the T-type calcium conductance (i.e. $g_T = 0$). When using the full spike train, we obtained directional bias values that were negative for low values of τ_{ON} (i.e. $\tau_{ON} < 0.1$ sec) and zero otherwise (Fig. 7A). In contrast, when using the burst train, we obtained directional bias values that were near zero when τ_{ON} was large (i.e. $\tau_{ON} > 0.2$ sec) and τ_{OFF} was small (i.e. $\tau_{OFF} < 0.2$ sec) and negative otherwise (Fig. 7B). The isolated spike train (Fig. 7C) tended to display directional bias values near zero except for low values of τ_{ON} (i.e. $\tau_{ON} < 0.02$ sec) and τ_{OFF} (i.e. $\tau_{OFF} < 0.2$ sec) where it was positive. As such, the ODI was zero for almost all values of τ_{ON} and τ_{OFF} except for low values of τ_{ON} (i.e. $\tau_{ON} < 0.02$ sec) and τ_{OFF} (i.e. $\tau_{OFF} < 0.2$ sec) for which it was negative (Fig. 7D). We also varied the gains G_{ON} and G_{OFF} and found qualitatively similar results in that the parameter regions for which opposite directional selectivity was observed were greatly reduced (compare Figs. S2 and S1).

The PSTH curves for the full spike train, bursts, and isolated spikes are shown for parameter values for which the ODI was negative and null in Figs. 7E and 7F, respectively. These values correspond to those indicated by the points "E" and "F" in Fig. 7D. In the regime where the opposite directional selectivity regime was observed, the firing rates from the full spike and burst trains were both greatest when the object moves from right to left while the maximum firing rate from the isolated spike train was greatest when the object moves from left to right (Fig. 7E). In contrast, in the regime where no directional selectivity was observed, the maximum firing rates of the full, burst, and isolated spike trains were all approximately equal for both movement directions (Fig. 7F).

We next plotted the directional biases of the full (Fig. 8A), burst (Fig. 8B), and isolated (Fig. 8C) spike trains as a function of both the bias current I_{bias} and the ratio of the synaptic depression time constants τ_{OFF}/τ_{ON} when $g_T = 0$. Our results show that the bias current I_{bias} can significantly influence movement direction coding by the full, burst, and isolated spike trains (Figs. 8A, B, C). Indeed, both the full spike (Fig. 8A) and burst (Fig. 8B) trains displayed similar profiles: no directional selectivity was observed for low values of τ_{OFF}/τ_{ON} (i.e. $\tau_{OFF}/\tau_{ON} < 3$) and negative directional biases were observed for higher values. In contrast, the isolated spike train (Fig. 8C) displayed a qualitatively different profile in that negative directional biases where observed for high values of τ_{OFF}/τ_{ON} (i.e. $\tau_{OFF}/\tau_{ON} > 10$) and low bias current values (i.e. $I_{bias} < 3.1$ nA) while positive values were observed for larger bias current values (i.e. $I_{bias} > 3.1$ nA) (Fig. 8C). As a result, the opposite directional selectivity index ODI displayed both positive and negative values when plotted as a function of I_{bias} and τ_{OFF}/τ_{ON} (Fig. 8D). As such, we observed both same and opposite direction selectivity regimes in our model without the T-type conductance.

The PSTH curves for the full spike train, bursts, and isolated spikes are shown for example same and opposite direction selectivity regimes in Figs. 8E and 8F, respectively. The parameter values used for the same and opposite direction selectivity regimes

are shown in Fig. 8D as points "E" and "F", respectively. For the same direction selectivity regime, the maximum firing rate from the full spike, burst, and isolated spike trains is strongest when the object moves from right to left (Fig. 8E). On the other hand, for the opposite directional selectivity regime, the maximum firing rate for the full spike and the burst trains are higher when the object moves from right to left while that of isolated spikes is highest when the object moves from left to right (Fig. 8F).

These results show that bursting mediated by T-type calcium channels is not necessary to observe opposite direction selectivity. However, such bursting greatly extends the range of values of the synaptic time constants τ_{ON} and τ_{OFF} and the bias current I_{bias} for which such coding is observed. We also note that the magnitude of directional biases observed for either of the full, burst, and isolated spike trains was smaller overall without the T-type conductance (compare Figs. 5 and 7 as well as Figs. 6 and 8). We conclude that T-type calcium channels promote movement coding by bursts and isolated spikes.

Electrosensory midbrain neurons display opposite coding of movement direction by bursts and isolated spikes

Our analysis of the effects of different parameters on movement direction coding by bursts and isolated spikes has shown the existence of regimes for which bursts and isolated spikes code for the same movement direction and regimes for which bursts and isolated spikes code for opposite movement directions. In order to test this prediction, we performed extracellular recordings from $N = 32$ TS neurons *in vivo* while moving an object back and forth along the rostro-caudal axis of the animal as done previously [18,26,35,62] (see Materials and Methods). We found that bursts and isolated spikes could code for opposite movement directions in 3 neurons. The PSTH obtained for the full, burst, and isolated spike trains for these three neurons are shown in Figs. 9A, 9B, 9C. We found that opposite coding of movement direction by bursts and isolated spikes was most pronounced for the neuron from Fig. 9C. Indeed, this neuron responded mostly with bursts when the object moved from tail to head and responded mostly with isolated spikes when the same object moved from head to tail (Fig. 9C). This was reflected in the directional biases from the burst and isolated spike trains that were 0.6, and -0.63, respectively. As such, bursts and isolated spikes displayed directional biases that were almost equal in magnitude for this neuron. These data suggest that there exists neurons in TS for which bursts and isolated spikes can code for opposite movement directions.

Decoding isolated spikes using a delay mechanism coupled with inhibition

Any information carried by action potential patterns such as bursts and isolated spikes is only functionally relevant if it is decoded by downstream neurons. We have previously proposed a biologically plausible circuitry for extracting burst spikes [26]. However, plausible neural circuits that can selectively respond to isolated spikes but are insensitive to bursts have not been proposed to date. We note that the ISI threshold criterion that we have used to separate bursts and isolated spikes is acausal in nature This is because any given spike can only be classified as being part of a burst based on whether the next spike occurs after an interval of time that is less than the burst threshold. Similarly, any given spike can only be classified as isolated if the next spike occurs after an interval of time that is greater than the burst threshold.

A schematic of a biophysically plausible neural circuit that is sensitive to isolated spikes is shown in Figure 10A (see Materials
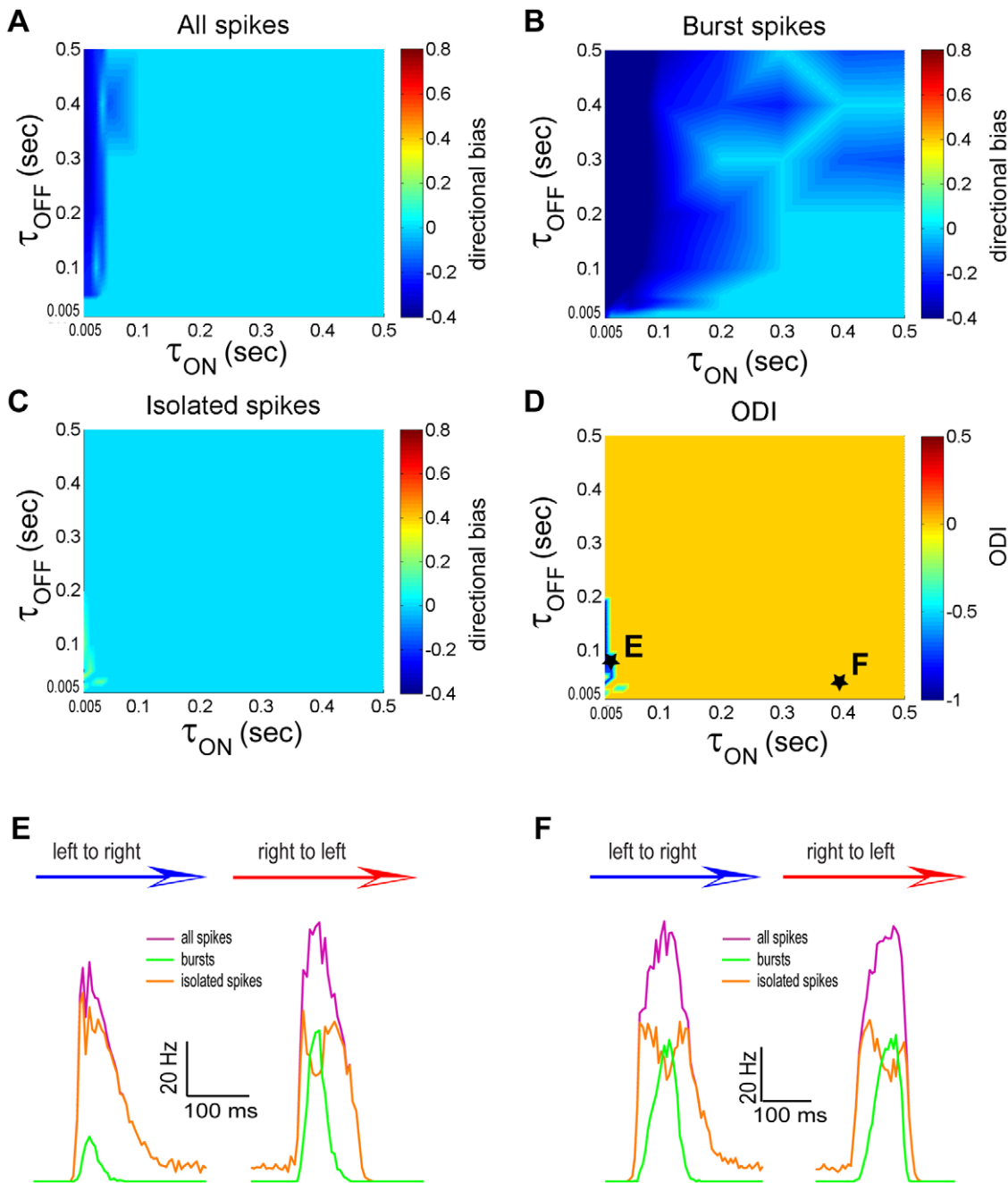
Figure 7. The synaptic depression time constants τ_{ON} and τ_{OFF} influence movement direction coding by bursts and isolated spikes with $g_T = 0$. A) Directional bias computed from the full spike train as a function of τ_{ON} and τ_{OFF}. **B**) Directional bias computed from the burst spike train as a function of τ_{ON} and τ_{OFF}. **C**) Directional bias computed from the isolated spike train as a function of τ_{ON} and τ_{OFF}. **D**) Opposite direction selectivity index as a function of τ_{ON} and τ_{OFF}. **E**) PSTH values near the maximum values in the left to right (blue arrow) and right to left (red arrow) directions for the full spike (purple), burst (green), and isolated (orange) spike trains for an example data point marked with a star in panel D. **F**) PSTH values near the maximum values in the left to right (blue arrow) and right to left (red arrow) directions for the full spike (purple), burst (green), and isolated (orange) spike trains for another example data point marked with a star in panel D.
doi:10.1371/journal.pone.0040339.g007

and Methods). It consists of two synapses: the first is excitatory and displays no synaptic plasticity (i.e. the EPSP amplitude elicited by each presynaptic action potential is the same), and the second is inhibitory and displays strong short-term facilitation. The second synapse, therefore, responds preferentially to bursts as shown previously [26]. The output of the excitatory synapse is delayed with respect to the output of the inhibitory synapse, and both

inputs are then summed and half-wave rectified (Fig. 10A). Intuitively, this circuit should be sensitive to isolated spikes for the following reason: bursts will give rise to greater facilitation of the inhibitory synapse, thereby causing a larger inhibition in the postsynaptic cell that will tend to prevent a response to the bursts from the excitatory synapse due to the delay. In contrast, isolated spikes will not induce such facilitation. As a result the inhibition is
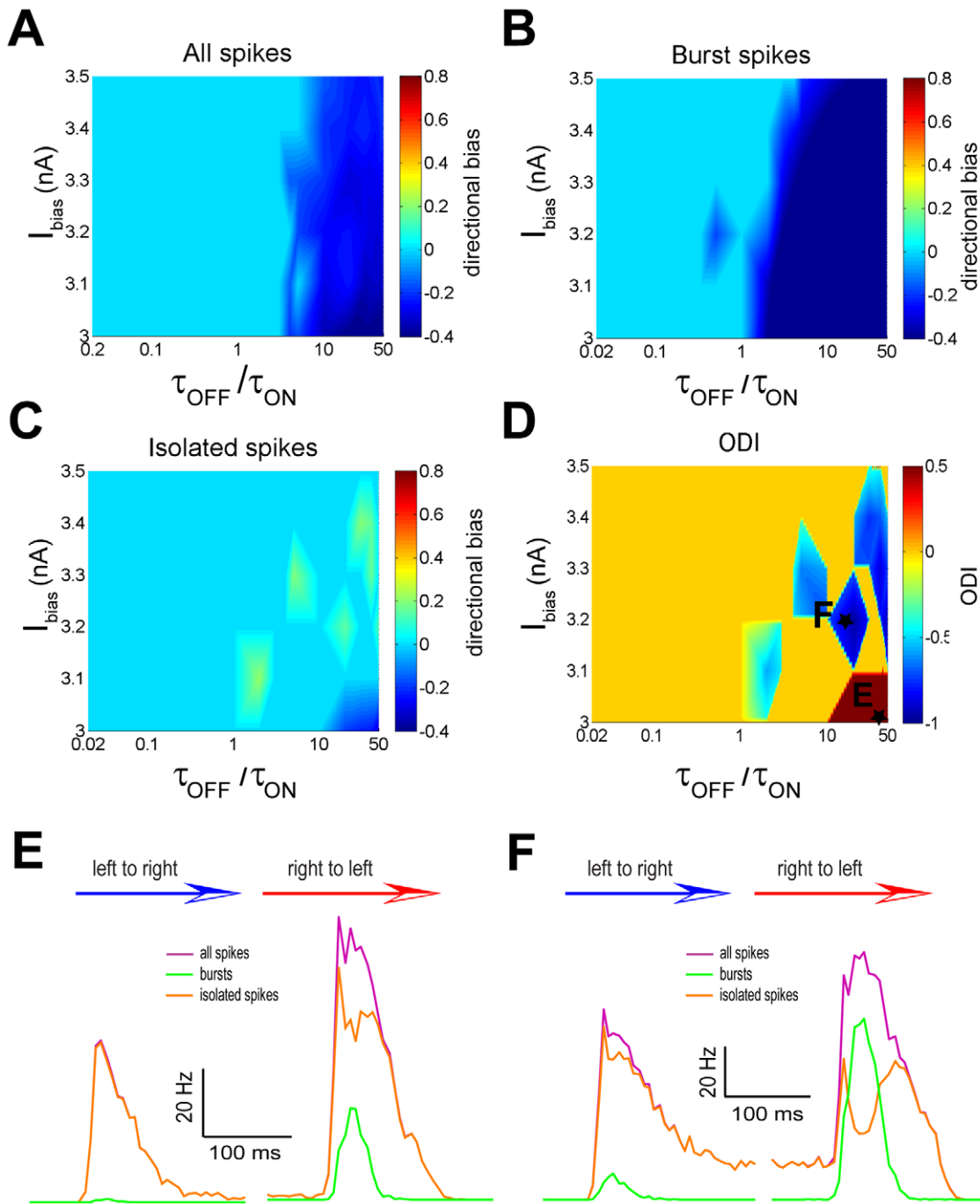
Figure 8. The bias current I$_{bias}$ and synaptic depression time constant ratio τ_{OFF}/τ_{ON} influence movement direction coding by bursts and isolated spikes with g$_T$ = 0. A) Directional bias computed from the full spike train as a function of τ_{OFF}/τ_{ON} and I$_{bias}$. **B**) Directional bias computed from the burst train as a function of τ_{OFF}/τ_{ON} and I$_{bias}$. **C**) Directional bias computed from the isolated spike train as a function of τ_{OFF}/τ_{ON} and I$_{bias}$. **D**) Opposite direction selectivity index as a function of τ_{OFF}/τ_{ON} and I$_{bias}$. **E**) PSTH values near the maximum values in the left to right (blue arrow) and right to left (red arrow) directions for the full spike (purple), burst (green), and isolated (orange) spike trains for an example data point marked with a star in panel D. **F**) PSTH values near the maximum values in the left to right (blue arrow) and right to left (red arrow) directions for the full spike (purple), burst (green), and isolated (orange) spike trains for another example data point marked with a star in panel D.
doi:10.1371/journal.pone.0040339.g008

sufficiently low such that the excitation from the first synapse can reach threshold for spiking. We note that such a scheme is not unreasonable since inhibition can sometimes precede excitation in midbrain neural circuits [63,64].

We next tested the performance of this simple model in segregating isolated spikes from bursts to that of an ISI threshold.

Our results show that this model was accurate at detecting isolated spikes (Fig. 10B). The spikes that were incorrectly classified tended to be the first spikes of bursts as determined by the ISI threshold that occurred after a period of isolated spiking, as the inhibition is then too weak and too short to block these (Fig. 10B). We then quantified this performance by using signal detection theory [65]
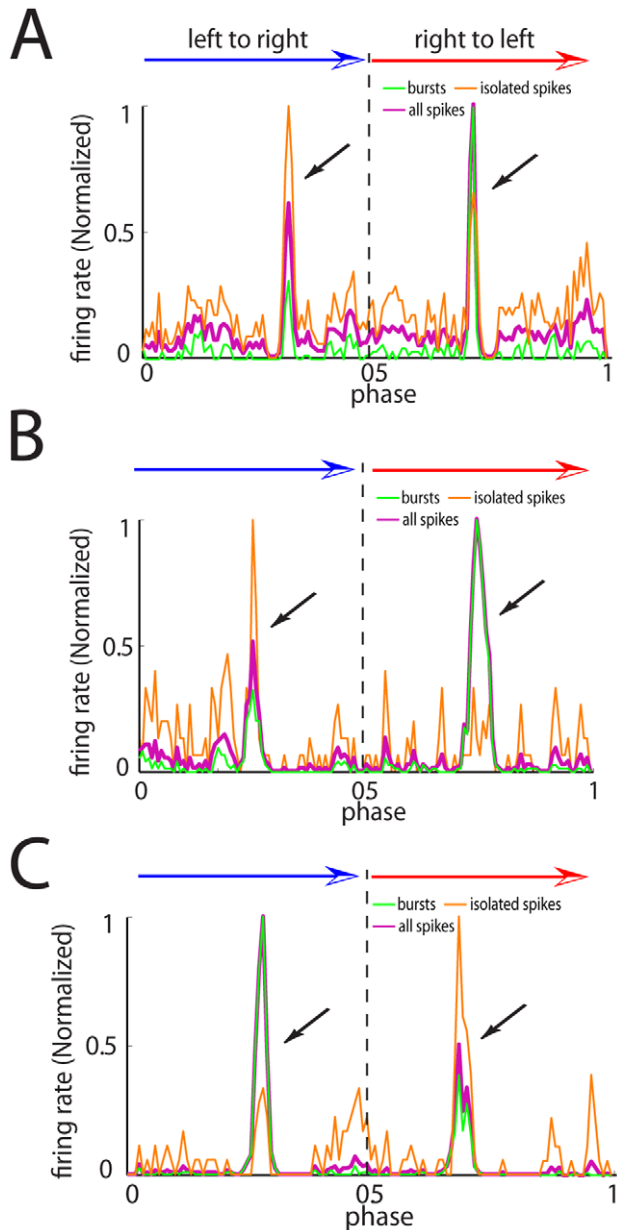
Figure 9. Electrosensory midbrain neurons can display opposite movement direction coding by bursts and isolated spikes.
A) Peri-stimulus time histogram (PSTH) for an example neuron computed from all spikes (purple), bursts (green), and isolated spikes (orange). The curves have been normalized by their maximum values. Directional bias (DB) values were −0.64, −0.39, and 0.36 for burst, all spikes, and isolated spikes, respectively. **B**) PSTH for another example neuron computed from all spikes (purple), bursts (green), and isolated spikes (orange). The curves have been normalized to 1. Directional bias (DB) values were −0.59, −0.5, and 0.56 for burst, all spikes, and isolated spikes, respectively. **C**) PSTH for another example neuron computed from all spikes (purple), bursts (green), and isolated spikes (orange). The curves have been normalized to 1. Directional bias (DB) values were 0.6, 0.5, and −0.63 for burst, all spikes, and isolated spikes, respectively.
doi:10.1371/journal.pone.0040339.g009

(see Materials and Methods) and found that this model gave high probabilities of correct classification for a wide range of delay t_d and synaptic facilitation time constant τ_F values (Fig. 11A). We also investigated whether the incorrectly classified spikes actually belonged to bursts and isolated spikes as determined by the ISI

threshold. To do so, we plotted the probability of misclassification for spikes that, according to the ISI threshold, were considered isolated spikes (Fig. 11B), the first spike of a burst (Fig. 11C), or any other spike of a burst (Fig. 11D). Thus, our results show that, for the parameter values that gave rise to the maximum probability of correct classification, the majority ($\approx 90\%$) of spikes that were incorrectly classified were actually the first spikes of a burst for the reason mentioned above. We found that these percentages strongly depended on parameter values (Figs. 11B, C, D). For example, increasing the delay for a given value of the facilitation time constant reduces the percentage of misclassified first spikes of a burst (Fig. 11C), increases the percentage of misclassified isolated spikes (Fig. 11B), and does not affect the remaining percentage of misclassified spikes that are part of a burst (Fig. 11D), but decreases the probability of correct classification (Fig. 11A).

We next varied both the inhibition time constant τ_I and gain G_I in our model. Our results show that the maximum probability of correct classification could be obtained for a wide range of values (Fig. 11E). Again, for the parameter values that gave rise to maximum probability of correct classification, the majority of misclassified spikes were actually the first spikes of bursts as seen by plotting the percentage of misclassified spikes that were considered isolated spikes (Fig. 11F), the first spike of a burst (Fig. 11G), or any other spike of a burst (Fig. 11H).

We next tested whether the extracted isolated spikes could indeed code for the opposite movement direction than that coded by both the burst and full spike trains, as observed using an ISI threshold. As such, we used the spiketrain from the example neuron shown in Fig. 9B as an input to the model. We found that the input and output PSTHs were maximal for opposite movement directions (Fig. 12A) and thus displayed opposite directional biases (Fig. 12B). Finally, we computed the directional bias of isolated spikes obtained with our model against that computed from isolated spikes obtained with the ISI threshold criterion across our experimental dataset (Fig. 12C) and observed a significant positive correlation between both quantities (R = 0.52, p = 0.0023, N = 32). These results show that a generic circuit with a temporal delay can be used to selectively extract directional information carried by isolated spikes.

Discussion

Summary of results

We have explored the coding of movement direction by specific action potential patterns, namely bursts and isolated spikes, in a biophysical model of directional selectivity in midbrain neurons of weakly electric fish. We found that, for a wide range of parameter values, bursts displayed strong directional selectivity and isolated spikes displayed little or no directional selectivity consistent with previous findings [26]. However, we also found a qualitatively different regime for which bursts and isolated spikes were preferentially elicited when the object moved in opposite directions. As such, our results show for the first time that bursts and isolated spikes can code for opposite movement directions. We have also shown that subthreshold T-type calcium channels can greatly enhance the range of parameter values for which this regime was observed. This is because such channels must be de-inactivated by inhibition in order to be activated by subsequent excitation and give rise to a burst of action potentials. We have also shown experimental recordings from TS neurons in weakly electric fish for which bursts and isolated spikes coded for opposite movement directions. Finally, we have shown that plausible simple neural circuits can reliably extract isolated spikes from spike trains that consist of both bursts and isolated spikes. To our knowledge,
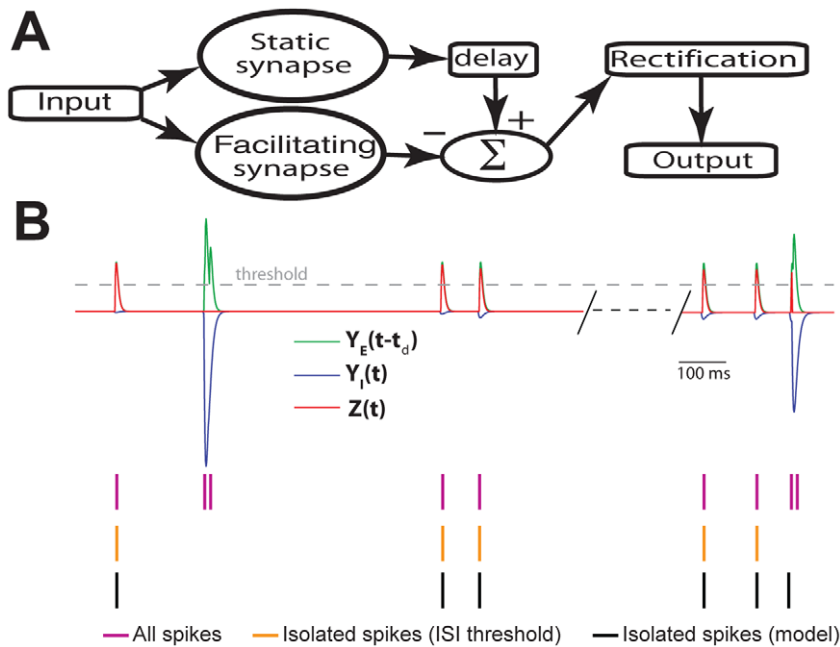
Figure 10. A biophysically plausible neural circuit can accurately extract isolated spikes and therefore decode their information about movement direction. A) Schematic of the decoding model for isolated spikes. It consists of parallel processing by two synapses with one displaying facilitation and the other displaying no plasticity (i.e. "static"). The output from the static synapse $Y_E(t)$ is delayed and the output from the facilitating synapse $Y_I(t)$ is then subtracted from it. This signal is then half-wave rectified to give the output $Z(t)$. Finally, $Z(t)$ is thresholded to obtain the output spikes. **B)** Performance of the decoding model compared with the performance of an ISI threshold criterion at detecting isolated spikes. Shown are the delayed output of the static excitatory synapse $Y_E(t-t_d)$ (green trace), facilitating inhibitory synapse $Y_I(t)$ (blue trace), and the output of the model $Z(t)$ (red trace) with the threshold used to detect output spikes (dashed gray trace), the original spike train (purple ticks), the isolated spikes according to the ISI threshold (orange ticks), and the isolated spikes according to the decoding model (black ticks). Parameter values used were $\tau_F = 200$ msec, $\tau_D = 500$ msec, $\tau_E = 5$ msec, $\tau_I = 8$ msec, $G_I = 5$, $I_0 = 3.41$ msec, $t_d = 4$ msec.
doi:10.1371/journal.pone.0040339.g010

these results constitute the first demonstration that bursts and isolated spikes can both code for movement direction in the same neuron. The relative simplicity and generality of our mathematical model suggests that our results will be applicable to other systems.

Role of active burst dynamics in generating directional selectivity

Previous studies have shown that, for most TS neurons, bursts and isolated spikes were the most and least reliable indicators of motion direction, respectively [26]. Therefore, it was suggested that isolated spikes coded for stimulus attributes other than motion direction. In this study we have shown that, for some TS neurons, bursts and isolated spikes can code for opposite movement directions. Our model predicts that an active burst mechanism mediated by a T-type calcium conductance is not necessary in order to observe opposite coding of movement direction by bursts and isolated spikes. Nevertheless, this active burst mechanism greatly extended the range of parameter values for which we observed this regime and moreover increased the degree of directional selectivity as quantified by the directional bias associated with the burst and isolated spike trains to values that were observed experimentally. The fact that we only observed this regime in a few TS neurons suggests that such neurons are quite rare, which most likely explains why these neurons were not found in previous studies [26]. Further studies using intracellular recordings are needed in order to test whether these neurons constitute a specific class within the TS that would thus be distinct from neurons for which bursts and isolated spikes code for the same movement direction and whether they selectively express T-type calcium channels as predicted from our model.

Functional relevance of opposite directional selectivity of bursts and isolated spikes

What is the functional relevance of having bursts and isolated spikes encode opposite movement direction in the same neuron? We propose that such parallel encoding may be used to discriminate different objects moving in opposite directions within the neuron's receptive field. Such parallel coding is entirely consistent with an emerging general picture in which bursts and isolated spikes can code for different stimulus attributes simultaneously and in parallel in the same neuron [25,39,41,42,44,52,66,67]. In weakly electric fish, foreground and background motion in opposite directions could occur during prey capture [10] or during tracking behavior [5] and the simultaneous encoding of both fore and background movement may be necessary for proper motor control.

Extracting bursts and isolated spikes

Our results are consistent with a growing body of literature that shows that bursts and isolated spikes can encode different stimulus attributes and thus might serve different functions [25,41,42,44,66,68,69]. This assumes that downstream neural circuits can somehow extract bursts and isolated spikes from a spike train. While previous studies have considered neural circuits that can selectively extract bursts [26,41,51,70], we are not aware of any previous studies that have proposed biophysically plausible neural circuits that would be sensitive exclusively to isolated spikes prior to this one.

Specifically, we have proposed that the neural circuits that would respond exclusively to isolated spikes need to include a delay. This delay is necessary because any given spike cannot be
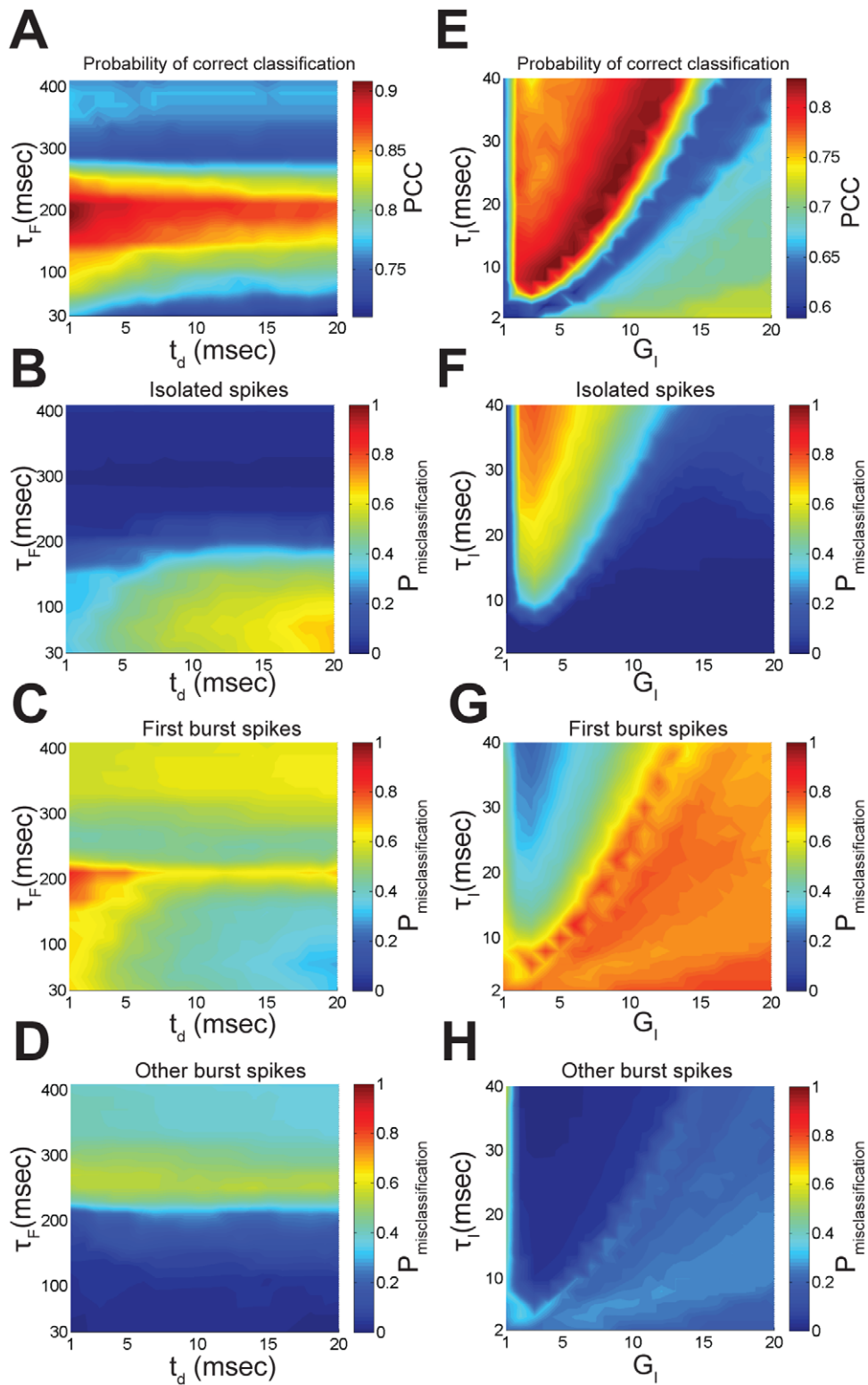
Figure 11. Extracting isolated spikes using a biologically plausible model. A) Probability of correct classification PCC as a function of the facilitation time constant τ_f and delay t_d. **B, C, D** Probability of misclassification $P_{misclassification}$ for the spikes that, according to the ISI threshold, were considered to be isolated spikes (**B**), the first spikes of a burst (**C**), or any other spikes of a burst (**D**), as a function of the facilitation time constant τ_f and delay t_d. Other parameter values used were $\tau_D = 500$ msec, $\tau_E = 5$ msec, $\tau_I = 5$ msec, $G_I = 7$, $I_0 = 3.41$ msec. **E**) Probability of correct classification PCC as a function of the inhibition time constant τ_I and gain G_I. **F, G, H** Probability of misclassification $P_{misclassification}$ for the spikes that, according to the ISI threshold, were considered to be isolated spikes (**F**), the first spikes of a burst (**G**), or any other spikes of a burst (**H**), as a function of the inhibition time constant τ_I and gain G_I. Other parameter values used were $\tau_F = 200$ msec, $\tau_D = 500$ msec, $\tau_E = 5$ msec, $I_0 = 3.41$ msec, $t_d = 4$ msec.
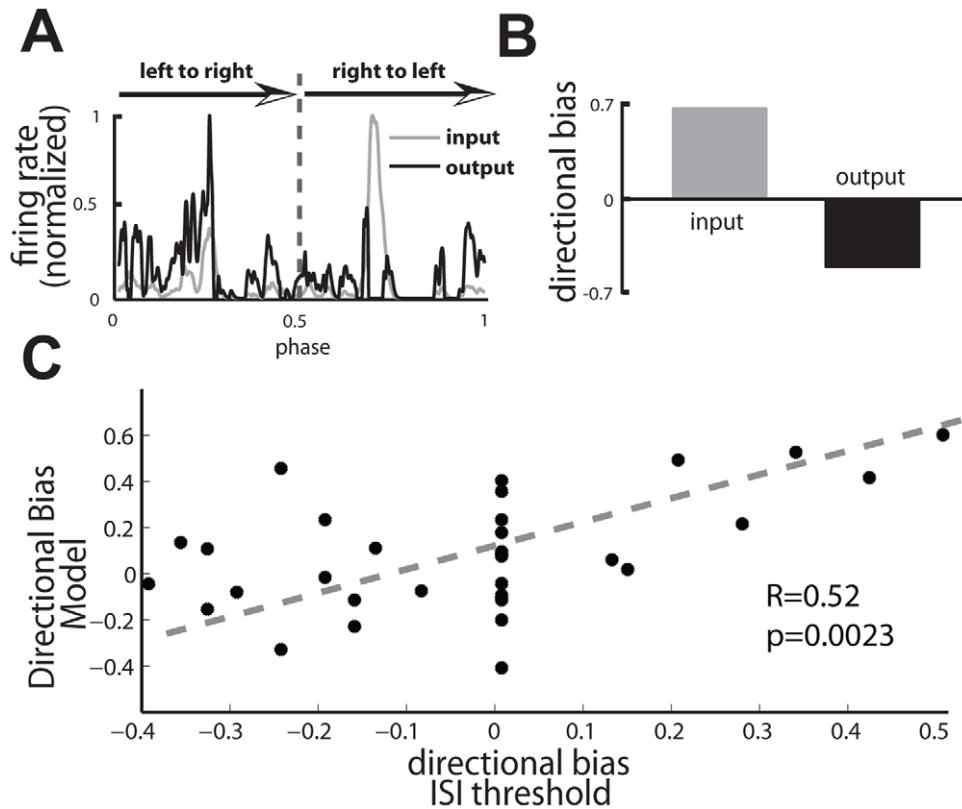doi:10.1371/journal.pone.0040339.g011

Figure 12. Comparison of a biologically plausible model with the ISI threshold. A) Input PSTH (gray) and output PSTH (black) from the model when the input consists of the full spike train from an example TS neuron. **B**) Output directional bias (black) and input directional bias (gray) computed from the PSTHs in C. Note the difference in sign. **C**) Directional bias of isolated spikes computed from the decoding model as a function of the directional bias of isolated spikes computed from the ISI threshold criterion. There was a significant positive correlation between both quantities (R = 0.52, p = 0.0023, N = 32). Parameter values used were $\tau_F = 70$ msec, $\tau_D = 500$ msec, $\tau_E = 5$ msec, $\tau_I = 8$ msec, $G_I = 7$, $I_0 = 3.41$ msec, $t_d = 4$ msec.
doi:10.1371/journal.pone.0040339.g012

unambiguously assigned as being part of a burst or being isolated without knowing at what time the next action potential will occur. Thus, it is necessary to compare the spike train at the present with the same spike train delayed by a time interval on the order of the burst threshold.

We note that neural circuits that use temporal combinations of delayed excitation and inhibition in order to achieve response selectivity have been described in other midbrain circuits and may be a general feature of sensory processing [63,64,71,72]. In *Apteronotus leptorhynchus*, many TS neurons project to the optic tectum (OT) where neurons respond selectively to moving objects in a directionally biased fashion [4,73]. It is possible that plasticity at the TS-OT synapses or a combination of excitation and inhibition from TS might enable OT neurons to decode bursts and/or isolated spikes from TS neurons. Future studies should investigate this interesting possibility.

Implications for other systems

Our results show that the traditional method for measuring directional selectivity, in which the maximum firing rates elicited in response to the moving object in each direction are compared, can in some cases fail to capture salient information transmitted by direction selective neurons. This is because such techniques take the full spike train into account. Indeed, we found parameter regimes for which the isolated and full spike trains displayed selectivity for opposite movement directions. Moreover, for subsets of these parameters, the full spike train displayed little

directional selectivity but for which the burst and isolated spike trains displayed opposite directional selectivity (see e.g. Fig. 6).

This result may have important consequences for the generation of direction selectivity in the mammalian visual cortex. Indeed, the electrosensory system has many parallels with thalamocortical pathways [74]. In particular, thalamic relay neurons within the lateral geniculate nucleus (LGN) have subthreshold T-type calcium channels that mediate burst firing [45,59,60,75–80]. The spike trains from thalamic relay neurons consist of a mixture of bursts and isolated spikes in the awake-behaving animals [42,81,82]. While previous studies have shown that these neurons are not directionally selective [12], these did not consider action potential patterns such as bursts and isolated spikes. We hypothesize that bursts of action potentials from thalamic relay neurons in LGN carry specific directional information that is then used by postsynaptic neurons within the primary visual cortex to generate directionally biased responses. This hypothesis is supported by the fact that thalamocortical synapses display strong depression and that sustained isolated action potential firing from thalamic relay neurons activates this depression [45,60,83]. Nevertheless, ~100 ms of inhibition can remove this depression as well as deinactivate T-type calcium channels. A subsequent depolarization caused by excitation can thus cause burst firing as well as an amplified post-synaptic response [45,60,83]. Studies performed within the LGN are necessary to validate this hypothesis and are beyond the scope of this paper.

Conclusion

We investigated whether action potential patterns such as bursts and isolated spikes encoded movement direction in a model of directional selectivity in electrosensory midbrain neurons. We found parameter regimes in which bursts and isolated spikes could encode opposite movement directions in the same neuron even though the full spike train displays little or no directional selectivity. As such, neurons that are categorized as non-directionally selective using the full spike train may in fact be highly directional selective if one considers instead particular action potential patterns. Such coding of opposite movement directions by bursts and isolated spikes could be used in discriminating different objects moving in opposite directions within the neuron's receptive field and is likely to be found across sensory systems.

Materials and Methods

Ethics statement

McGill University's institutional Animal Care and Use Committee approved all experimental procedures and animal husbandry.

Animals

We used the weakly electric fish *Apteronotus leptorhynchus* in this study. Animals were obtained from tropical fish suppliers and were housed in laboratory tanks for several days in order to become acclimated to the new environment. This was performed according to published guidelines [84]. The surgical and experimental procedures have been described in detail elsewhere [18,35,62,85–88].

Stimulation and recording

Extracellular recordings from TS neurons were made using previously described techniques [18,35,62,89]. We used both patch [62,89] and metal-filled micropipettes [62,90–92] to obtain these recordings. The stimulus consisted of a 1.8 cm wide metal plate coated with a plastic coating on the side opposite to the animal that was actuated using a pen plotter (HP 7010B). This object moved back and forth along the animal's rostro-caudal axis over a distance of 20 cm [17,18,35,93,94] for at least 30 cycles. The sinusoid was centered at the animal's midpoint and had a frequency of 0.25 Hz, corresponding to an average velocity of ∼10 cm/sec. These velocities correspond to those that the animal experiences during prey capture [10] and within the velocities of error signals observed during refuge tracking [5].

Data were acquired with a Cambridge Electronic Design Power1401 hardware and Spike2 software (Cambridge, UK) and analyzed using Spike2 (CED) and custom-made routines in MATLAB (The Mathworks, Natick, MA). The recorded membrane potentials were thresholded in order to obtain the action potential times. We excluded neurons whose total spike count was less than 400 over the stimulus duration. Recorded spike trains were segregated into bursts and isolated spikes as described above using an ISI threshold. Neurons with burst or isolated spike counts less than 100 were not analyzed.

Burst and isolated spike classification

We used an interspike interval threshold to separate the simulated spiking responses into burst and isolated spikes [25,36,41,44] (Fig. 1D). Specifically, two consecutive action potentials that were separated by a time interval less than the burst threshold were considered as part of a burst. Spikes that were not part of bursts were included in the isolated spike train. The burst threshold was computed as the time at which the falling

phase of initial peak of the autocorrelogram crossed the 99.9% Poisson confidence limit as done previously [25,26,36,95].

Quantifying directional selectivity and opposite directionality

The full spike, burst (i.e. the train of spikes that belong to bursts) and the isolated (i.e. the train of spikes that are isolated) spike trains were each used to compute peri-stimulus time histograms (PSTHs) in response to the moving object. We then computed a measure of directional bias as [18,35]:

$$DB = \frac{R_{LR} - R_{RL}}{\max(R_{LR}, R_{RL})}$$

where R_{LR}, R_{RL} are the maximum firing rates obtained when the object moves from "left to right" and "right to left", respectively (note that "left to right" corresponds to the object moving from the animal's snout to the tail and that "right to left" corresponds to the object moving from the tail to the snout) and max(R_{LR}, R_{RL}) is the maximum of the two. This measure varies between -1 and 1. DB values of 1 and -1 indicate complete direction preference for movement from left to right and from right to left, respectively, while a value of 0 indicates no direction selectivity.

To quantify the opposite directionality we used the directional biases computed from burst spikes and isolated spikes and then computed the opposite directionality index as:

$$ODI = i|DB_{burst} - DB_{isolatedspikes}|$$

where i is 1 if the maximum firing rate of burst spikes and isolated spikes happen preferentially for the same object movement direction and is -1 otherwise. i is 0 if directional biases of bursts or isolated spikes equal 0.

Modeling TS neurons

Our model TS neuron's one-dimensional receptive field consists of two 10 mm long adjacent 'ON' and 'OFF' zones. The 'ON' zone represents the output of E-type ELL pyramidal cells that are excited by the stimulus while the 'OFF' zone represents the output of I-type ELL pyramidal cells that are inhibited by the stimulus as observed experimentally [85,96]. Then a point object moved at a speed of 10 cm/s back and forth across these zones. The output of each zone is then given by [18]:

$$O_i(t) = F_i + v_i G_i \Theta(t - \lambda_i) exp\left(-\frac{t - \lambda_i}{\tau_i}\right)$$

where F_i is the bias current which represents the baseline activity from E and I-type pyramidal cells which are approximately equal on average [97,98] and $v_i = 1, -1$ for i = ON, OFF, respectively. Here τ_i is the depression time constant associated with zone i, λ_i is the time that object enters zone i, and G_i is the gain of zone i. The responses of each zone were then convolved with an alpha function with time constant 20 msec to mimic synaptic EPSPs. Consistent with anatomical data showing that both E and I-type ELL pyramidal neurons make excitatory connections onto TS neurons [99], the input I(t) to our neuron model is taken to be:

$$I(t) = O_{ON} + O_{OFF}$$

We note that the outputs from the ON and OFF zone, O_{ON} and O_{OFF}, were not delayed with respect to one another, which is consistent with recent experimental results showing no significant delay between the inputs from E and I-type sources onto TS neurons [88]. The TS neuron was modeled using the Hodgkin-Huxley formalism based on available experimental data [35], the model contains spiking sodium, delayed rectifier potassium, low threshold calcium (T-type), and leak conductances:

$$C\frac{dV}{dt} = -g_{leak}(V - E_{leak}) - g_T s_\infty^3(V)h(V - E_{Ca})$$
$$- g_{Na}m_\infty^3(V)(0.85 - n)(V - E_{Na}) - g_K n^4(V)(V - E_K)$$
$$+ A\,I(t) + I_{bias} + \sigma\,\xi(t)$$

$$\frac{dh}{dt} = \Phi\frac{h_\infty(V) - h}{\tau_h(V)}$$

$$\frac{dn}{dt} = \frac{n_\infty(V) - n}{\tau_n(V)}$$

$$m_\infty(V) = \frac{\alpha_m(V)}{\alpha_m(V) + \beta_m(V)}$$

$$n_\infty(V) = \frac{\alpha_n(V)}{\alpha_n(V) + \beta_n(V)}$$

$$\tau_n(V) = \frac{0.05}{\alpha_n(V) + \beta_n(V)}$$

$$\alpha_m(V) = \frac{0.1\,(V + 40.7)}{1 - exp[-0.1\,(V + 40.7)]}$$

$$\beta_m(V) = 4\,exp[-0.05\,(V + 49.7)]$$

$$\alpha_n(V) = \frac{0.01\,(V + 40.7)}{1 - exp[-0.1\,(V + 40.7)]}$$

$$\beta_n(V) = 0.125\,exp[-0.0125\,(V + 50.7)]$$

$$s_\infty(V) = \frac{1}{1 + exp[-(V + 69)/7.8]}$$

$$h_\infty(V) = \frac{1}{0.5 + \sqrt{0.25 + exp[(V + 82)/6.3]}}$$

$$\tau_h(V) = 30 + \frac{exp[(V + 150)/18]}{1.5 + \sqrt{0.25 + exp[(V - 70)/4]}}$$

where C is the membrane capacitance, V is the transmembrane potential difference, g_{leak} is the leak conductance with reversal potential E_{leak}. Here g_T, g_{Na}, and g_K are the voltage-gated calcium, sodium, and potassium conductances with reversal potentials E_{Ca}, E_{Na}, and E_K, respectively. A is the synaptic weight and I_{bias} is a constant bias current, $\sigma\xi(t)$ is zero mean low-pass filtered Gaussian white noise with standard deviation σ that mimics sources of synaptic input [100].

We simulated this model numerically using an Euler-Maruyama Algorithm with integration time step dt = 0.0025 msec. Other parameter values used, unless otherwise stated, were g_{leak} = 0.18 μS, g_T = 0.32 μS, g_{Na} = 30 μS, g_K = 10 μS, E_{leak} = −65 mV, E_{Ca} = 120 mV, E_{Na} = 60 mV, E_K = −85 mV, C = 1 μF, A = 0.75, B = 0.1, = 2, $G_1 = G_2 = 1$, I_{bias} = −1.3 nA, $G_{ON} = G_{OFF} = 1$, $F_{ON} = F_{OFF} = 2$, τ_{ON} = 5 msec, τ_{OFF} = 500 msec. These values are comparable to those used in previous modeling studies [35,59]. For some simulations, we set g_T = 0 and I_{bias} = 3.1 nA to adjust for firing rate. All simulations for computing PSTHs and directional

biases were done over 1000 trials. We explored the parameter spaces by systematically varying synaptic depression time constants of ON and OFF zones in a range of 5 msec to 500 msec which is biologically relevant [18]. To explore the effect of synaptic depression time constants and bias current together we used synaptic depression time constants ratio τ_{OFF}/τ_{ON} in the range of 1/50 to 50 in which τ_{OFF} and τ_{ON} were (in sec) [0.01 0.5], [0.01 0.4], [0.01 0.3], [0.01 0.3], [0.01 0.2], [0.01 0.1], [0.01 0.05], [0.01 0.04], [0.01 0.03], [0.01 0.02], [0.01 0.01], [0.02 0.01], [0.03 0.01], [0.04 0.01], [0.05 0.01], [0.1 0.01], [0.2 0.01], [0.3 0.01], [0.4 0.01], [0.5 0.01].

In all our analysis and figures in which the directional biases from our model were plotted as a function of parameters, directional biases whose magnitude was below 0.15 were set to zero. This is because previous analysis has shown that such directional biases were not significantly different from zero [18]. The burst threshold that was used for our model simulations was set at 10 msec as done previously [26].

Modeling biophysically plausible mechanisms to extract isolated spikes

While the interspike interval threshold procedure described above is a simple computational method for segregating bursts and isolated spikes, it is not clear how such a threshold mechanism could be implemented in CNS circuits. A neural circuit which responses to bursts and is insensitive to isolated spikes has been previously considered [26]. However, the complement problem of designing a neural circuit that would be unresponsive to bursts but sensitive to isolated spikes has, to our knowledge, not been considered before.

Here we introduce a plausible circuit that can extract isolated spikes. Specifically, we consider the presynaptic spike train as a sum of delta functions:

$$X(t) = \sum_{i=1}^{N} \delta(t - t_i),$$

where t_i is the ith spike time. X(t) is first passed through two parallel synapses. The first is excitatory and does not have any synaptic dynamics (i.e. no plasticity and the amplitude of the output EPSP is the same for all presynaptic action potentials), the output of this synapse is thus given by convolving the input spike train X(t) with an alpha function with time constant τ_E:

$$Y_E(t) = \sum_{i=1}^{N} \Theta(t - t_i)\frac{t - t_i}{\tau_E^2}exp\left(-\frac{t - t_i}{\tau_E}\right).$$

The second synapse is inhibitory and displays plasticity. This plasticity is described by facilitation and depression terms [101−104]:

$$\frac{dD}{dt} = \frac{1 - D}{\tau_D}; \quad t = t_i \Rightarrow D(t_i) \to D(t_i)(1 - F(t_i))$$

$$\frac{dF}{dt} = -\frac{F}{\tau_F}; \quad t = t_i \Rightarrow F(t_i) \to F(t_i) + \Delta F(t_i - t_{i-1})$$

$$\Delta F(I) = \frac{I_0}{I}$$

At the time of an input spike t_i, D is first decreased by an amount $F(t_i)D(t_i)$; then F is updated by an increment ΔF. The increment ΔF is inversely proportional to the time interval between the current action potential and the last one. As such, short time intervals such as those that occur during burst firing will cause more potentiation than longer ones. We have also introduced an upper bound for F (i.e. $F(t) \leq 1$) to prevent negative values for the update factor of the depression variable. The output of this synapse is thus given by:

$$Y_I(t) = -G_I \sum_{i=1}^{N} \Theta(t-t_i)D(t_i)F(t_i)\frac{t-t_i}{\tau_I^2}exp\left(-\frac{t-t_i}{\tau_I}\right),$$

where D, F are the depression and facilitation terms, respectively. Here τ_I is the time constant of the alpha function that models the time course of the IPSP and G_I is a gain term. As such, the inhibitory synapse displayed strong facilitation in response to a burst of presynaptic action potentials. We assume that the output $Y_E(t)$ is delayed by a time t_d. The postsynaptic output is then given by:

$$Z(t) = TF(Y_E(t-t_d) + Y_I(t)),$$

with TF defined as:

$$TF(Y) = \begin{cases} Y & if & Y \geq 0 \\ 0 & if & Y < 0 \end{cases}$$

The post-synaptic spike train was obtained by thresholding Z(t) (i.e. finding the times at which Z(t) crosses a threshold value from below). We then took experimentally recorded spike sequences, and segregated them into bursts and isolated spikes using both our decoding model and ISI threshold methods. Then, we compared the sequences of burst and isolated spikes obtained from each model in the following way. We used signal detection theory [65] in order to quantify the decoding model's performance at detecting isolated spikes as defined by the ISI threshold. We computed the probability of correct detection (P_D) as the fraction of spike times deemed to be part of isolated spike train according to the decoding model that were also deemed part of isolated spike train using the ISI threshold criterion (i.e. that were "correctly" classified). The probability of false alarm (P_{FA}) was computed as the fraction of spike times deemed to be part of isolated spike train according to the decoding model that were deemed to be burst using the ISI threshold criterion (i.e. that were "incorrectly" classified). The overall performance can then be quantified by computing the probability of correct classification (PCC) as:

$$PCC = \frac{P_D}{2} + \frac{(1-P_{FA})}{2}$$

A value of PCC = 0.5 implies that our model performs at chance level compared to the ISI threshold criterion (i.e. that any given spike is randomly assigned as being part of a burst or isolated). In contrast, PCC = 1 indicates that the model performs identically to the ISI threshold criterion. We note that this does not imply that the ISI threshold criterion is optimal in any way as segregating bursts and isolated spikes, merely that our biophysically plausible decoding model performs as well. As such, signal detection theory is used here to determine how well the decoding model performs relative to the ISI threshold criterion.

Supporting Information

Figure S1 The gains G_{ON} and G_{OFF} strongly influence movement direction coding by bursts and isolated spikes. A) Directional bias computed from the full spike train as a function of G_{ON} and G_{OFF}. **B**) Directional bias computed from the burst spike train as a function of G_{ON} and G_{OFF}. **C**) Directional bias computed from the isolated spike train as a function of G_{ON} and G_{OFF}. **D**) Opposite direction selectivity index (ODI) as a function of τ_{ON} and τ_{OFF}.
(TIF)

Figure S2 The gains G_{ON} and G_{OFF} influence movement direction coding by bursts and isolated spikes with $g_T = 0$. A) Directional bias computed from the full spike train as a function of G_{ON} and G_{OFF}. **B**) Directional bias computed from the burst spike train as a function of G_{ON} and G_{OFF}. **C**) Directional bias computed from the isolated spike train as a function of G_{ON} and G_{OFF}. **D**) Opposite direction selectivity index as a function of G_{ON} and G_{OFF}.
(TIF)

Acknowledgments

Author Contributions

Conceived and designed the experiments: MJC. Performed the experiments: NKH MJC. Analyzed the data: NKH. Contributed reagents/materials/analysis tools: NKH MJC. Wrote the paper: NKH MJC.

References

1. Tammero LF, Frye MA, Dickinson MH (2004) Spatial organization of visuomotor reflexes in Drosophila. J Exp Biol 207: 113−122.
2. Frye MA (2001) Effects of stretch receptor ablation on the optomotor control of lift in the hawkmoth Manduca sexta. J Exp Biol 204: 3683−3691.
3. Srinivasan MV, Poteser M, Kral K (1999) Motion detection in insect orientation and navigation. Vision Res 39: 2749−2766.
4. Rose GJ, Call SJ (1993) Temporal filtering properties of midbrain neurons in an electric fish: implications for the function of dendritic spines. Journal of Neuroscience 13: 1178−1189.
5. Cowan NJ, Fortune ES (2007) The critical role of locomotion mechanics in decoding sensory systems. Journal of Neuroscience 27: 1123−1128.
6. Horak FB, Macpherson JM (1996) Postural orientation and equilibrium. In: Rowell LB, Shepherd JT, editors. Handbook of physiology section 12: Exercise regulation and integration of multiple systems. New York (New York): Oxford University Press. 255–292.

7. Kuo AD (2005) An optimal state estimation model of sensory integration in human postural balance. J Neural Eng 2: S235−249.
8. Kiemel T, Oie KS, Jeka JJ (2002) Multisensory fusion and the stochastic structure of postural sway. Biol Cybern 87: 262−277.
9. Carver S, Kiemel T, van der Kooij H, Jeka JJ (2005) Comparing internal models of the dynamics of the visual environment. Biol Cybern 92: 147−163.
10. Nelson ME, MacIver MA (1999) Prey capture in the weakly electric fish Apteronotus albifrons: sensory acquisition strategies and electrosensory consequences. Journal of Experimental Biology 202: 1195−1203.
11. MacIver MA, Sharabash NM, Nelson ME (2001) Prey-capture behavior in gymnotid electric fish: motion analysis and effects of water conductivity. J Exp Biol 204: 543−557.
12. Hubel DH, Wiesel TN (1962) Receptive fields, binocular interaction and functional architecture in the cat's visual cortex. Journal of Physiology 160: 106−154.

13. Euler T, Detwiler PB, Denk W (2002) Directionally selective calcium signals in dendrites of starburst amacrine cells. Nature 418: 845−852.

14. Haag J, Denk W, Borst A (2004) Fly motion vision is based on Reichardt detectors regardless of the signal-to-noise ratio. PNAS 101: 16333–16338.

15. Heiligenberg W, Rose GJ (1987) The Optic Tectum of the Gymnotiform Electric Fish, Eigenmannia – Labeling of Physiologically Identified Cells. Neuroscience 22: 331–340.

16. Bastian J (1982) Vision and Electroreception – Integration of Sensory Information in the Optic Tectum of the Weakly Electric Fish Apteronotus-Albifrons. Journal of Comparative Physiology 147: 287–297.

17. Ramcharitar JU, Tan EW, Fortune ES (2006) Global Electrosensory Oscillations Enhance Directional Responses of Midbrain Neurons in Eigenmannia. Journal of Neurophysiology 96: 2319–2326.

18. Chacron MJ, Toporikova N, Fortune ES (2009) Differences in the Time Course of Short-Term Depression Across Receptive Fields Are Correlated With Directional Selectivity in Electrosensory Neurons. Journal of Neurophysiology 102: 3270–3279.

19. Borst A (2007) Correlation versus gradient type motion detectors: the pros and cons. Philosophical Transactions of the Royal Society of London – Series B: Biological Sciences 362: 369–374.

20. Derrington AM, Allen HA, Delicato LS (2004) Visual mechanisms of motion analysis and motion perception. Annu Rev Psychol 55: 181–205.

21. Hock HS, Schoner G, Gilroy L (2009) A counterchange mechanism for the perception of motion. Acta Psychol (Amst) 132: 1–21.

22. Maex R, Orban GA (1991) Subtraction inhibition combined with a spiking threshold accounts for cortical direction selectivity. Proc Natl Acad Sci U S A 88: 3549–3553.

23. Borst A, Egelhaaf M (1989) Principles of visual motion detection. Trends Neurosci 12: 297–306.

24. Borst A, Egelhaaf M (1990) Direction selectivity of blowfly motion-sensitive neurons is computed in a two-stage process. PNAS 87: 9363–9367.

25. Avila Akerberg O, Krahe R, Chacron MJ (2010) Neural heterogeneities and stimulus properties affect burst coding in vivo. Neuroscience 168: 300–313.

26. Khosravi-Hashemi N, Fortune ES, Chacron MJ (2011) Coding Movement Direction by Burst Firing in Electrosensory Neurons. Journal of Neurophysiology 106: 1954–1968.

27. Jagadeesh B, Wheat HS, Kontsevich LL, Tyler CW, Ferster D (1997) Direction selectivity of synaptic potentials in simple cells of the cat visual cortex. Journal of Neurophysiology 78: 2772–2789.

28. Priebe NJ, Ferster D (2008) Inhibition, spike threshold, and stimulus selectivity in primary visual cortex. Neuron 57: 482–497.

29. Priebe NJ, Mechler F, Carandini M, Ferster D (2004) The contribution of spike threshold to the dichotomy of cortical simple and complex cells. Nature Neuroscience 7: 1113–1122.

30. Reichardt W, Wenking H (1969) Optical detection and fixation of objects by fixed flying flies. Naturwissenschaften 56: 424–425.

31. Reichardt W (1987) Evaluation of optical motion information by movement detectors. Journal of Comparative Physiology A 161: 533–547.

32. Carver S, Roth E, Cowan NJ, Fortune ES (2008) Synaptic plasticity can produce and enhance direction selectivity. PLoS Computational Biology 4: e32.

33. Chance FS, Nelson SB, Abbott LF (1998) Synaptic depression and the temporal response characteristics of V1 cells. Journal of Neuroscience 18: 4785–4799.

34. Adelson EH, Bergen JR (1985) Spatiotemporal energy models for the perception of motion. Journal of the Optical Society of America A-Optics & Image Science 2: 284–299.

35. Chacron MJ, Fortune ES (2010) Subthreshold membrane conductances enhance directional selectivity in vertebrate sensory neurons. Journal of Neurophysiology 104: 449–462.

36. Chacron MJ, Bastian J (2008) Population coding by electrosensory neurons. Journal of Neurophysiology 99: 1825–1835.

37. Chacron MJ, Longtin A, Maler L (2001) Simple models of bursting and non-bursting electroreceptors. Neurocomputing 38: 129–139.

38. Chacron MJ, Longtin A, Maler L (2004) To Burst or Not to Burst? Journal of Computational Neuroscience 17: 127–136.

39. Deemyad T, Maler L, Chacron MJ (2011) Inhibition of SK and M channel mediated currents by 5-HT enables parallel processing by bursts and isolated spikes. Journal of Neurophysiology 105: 1276–1294.

40. Gabbiani F, Koch C (1996) Coding of Time-Varying Signals in Spike Trains of Integrate-and-Fire Neurons with Random Threshold. Neural Computation 8: 44–66.

41. Kepecs A, Lisman J (2003) Information encoding and computation with spikes and bursts. Network 14: 103–118.

42. Lesica NA, Stanley GB (2004) Encoding of natural scene movies by tonic and burst spikes in the lateral geniculate nucleus. Journal of Neuroscience 24: 10731–10740.

43. Martinez-Conde S, Macknik SL, Hubel DH (2002) The function of bursts of spikes during visual fixation in the awake primate lateral geniculate nucleus and primary visual cortex. PNAS 99: 13920–13925.

44. Oswald AMM, Chacron MJ, Doiron B, Bastian J, Maler L (2004) Parallel Processing of Sensory Input by Bursts and Isolated Spikes. Journal of Neuroscience 24: 4351–4362.

45. Sherman SM (2001) Tonic and burst firing: dual modes of thalamocortical relay. Trends in Neurosciences 24: 122–126.

46. Avila-Akerberg O, Krahe R, Chacron MJ (2010) Neural heterogeneities and stimulus properties affect burst coding in vivo. Neuroscience 168: 300–313.

47. Avila Akerberg O, Chacron MJ (2011) Nonrenewal spike train statistics: causes and functional consequences on neural coding. Experimental Brain Research 210: 353–371.

48. DeBusk BC, DeBruyn EJ, Snider RK, Kabara JF, Bonds AB (1997) Stimulus-dependent modulation of spike burst length in cat striate cortical cells. Journal of Neurophysiology 78: 199–213.

49. Eyherabide HG, Rokem A, Herz AV, Samengo I (2008) Burst firing is a neural code in an insect auditory system. Front Comput Neurosci 2: 3.

50. Gaudry KS, Reinagel P (2008) Information measure for analyzing specific spiking patterns and applications to LGN bursts. Network 19: 69–94.

51. Kepecs A, Wang XJ, Lisman J (2002) Bursting Neurons Signal Input Slope. Journal of Neuroscience 22: 9053–9062.

52. Marsat G, Pollack GS (2010) The structure and size of sensory bursts encode stimulus information but only size affects behavior. Journal of Comparative Physiology A 196: 315–320.

53. Oswald AM, Doiron B, Maler L (2007) Interval coding. I. Burst interspike intervals as indicators of stimulus intensity.[see comment]. Journal of Neurophysiology 97: 2731–2743.

54. Samengo I, Montemurro MA (2010) Conversion of phase information into a spike-count code by bursting neurons. PLoS One 5: e9669.

55. Chacron MJ, Longtin A, Maler L (2011) Efficient computation via sparse coding in electrosensory neural networks. Current Opinion in Neurobiology 21: 752–760.

56. Turner RW, Maler L, Burrows M (1999) Electroreception and electrocommunication. Journal of Experimental Biology 202: 1167–1458.

57. Hodgkin AL, Huxley AF (1952) A quantitative description of membrane current and its application to conduction and excitation in nerve. Journal of Physiology London 117: 500–544.

58. Carr CE, Maler L (1986) Electroreception in gymnotiform fish. Central anatomy and physiology. In: Bullock TH, Heiligenberg W, editors. Electroreception. New York: Wiley. 319–373.

59. Rush ME, Rinzel J (1994) Analysis of bursting in a thalamic neuron model. Biol Cybern 71: 281–291.

60. Sherman SM, Guillery RW (2006) Exploring the Thalamus and its Role in Cortical Function. Cambridge, MA: MIT Press.

61. Destexhe A, Rudolph M, Pare D (2003) The high-conductance state of neocortical neurons in vivo. Nature Reviews Neuroscience 4: 739–751.

62. Vonderschen K, Chacron MJ (2011) Sparse and dense coding of natural stimuli by distinct midbrain neuron subpopulations. Journal of Neurophysiology 106: 3102–3118.

63. Leary CJ, Edwards CJ, Rose GJ (2008) Midbrain auditory neurons integrate excitation and inhibition to generate duration selectivity: an in vivo whole-cell patch study in anurans. Journal of Neuroscience 28: 5481–5493.

64. Edwards CJ, Leary CJ, Rose GJ (2008) Mechanisms of long-interval selectivity in midbrain auditory neurons: roles of excitation, inhibition, and plasticity. Journal of Neurophysiology 100: 3407–3416.

65. Green D, Swets J (1966) Signal Detection Theory and Psychophysics. New York: John Wiley & Sons.

66. Marsat G, Proville RD, Maler L (2009) Transient signals trigger synchronous bursts in an identified population of neurons. Journal of Neurophysiology 102: 714–723.

67. Marsat G, Pollack GS (2004) Differential Temporal Coding of Rhythmically Diverse Acoustic Signals by a Single Interneuron. Journal of Neurophysiology 92: 939–948.

68. Avila Akerberg O, Chacron MJ (2011) In vivo conditions influence the coding of stimulus features by bursts of action potentials. Journal of Computational Neuroscience 31: 369–383.

69. Marsat G, Maler L (2010) Neural heterogeneity and efficient population codes for communication signals. Journal of Neurophysiology 104: 2543–2555.

70. Lisman JE (1997) Bursts as a unit of neural information: making unreliable synapses reliable. Trends in Neurosciences 20: 38–43.

71. George AA, Lyons-Warren AM, Ma X, Carlson BA (2011) A diversity of synaptic filters are created by temporal summation of excitation and inhibition. Journal of Neuroscience 31: 14721–14734.

72. Carlson BA (2009) Temporal-pattern recognition by single neurons in a sensory pathway devoted to social communication behavior. Journal of Neuroscience 29: 9417–9428.

73. Bastian J (1982) Vision and electroreception. Integration of sensory information in the optic tectum of the weakly electric fish Apteronotus Albibrons. Journal of Comparative Physiology A 147: 287–297.

74. Krahe R, Gabbiani F (2004) Burst Firing in Sensory Systems. Nature Reviews Neuroscience 5: 13–23.

75. Lu SM, Guido W, Sherman SM (1992) Effects of membrane voltage on receptive field properties of lateral geniculate neurons in the cat: contributions of the low-threshold Ca2+ conductance. Journal of Neurophysiology 68: 2185–2198.

76. Jahnsen H, Llinas R (1984) Electrophysiological properties of guinea-pig thalamic neurones: an in vitro study. Journal of Physiology (London) 349: 205–226.

77. Sherman SM, Guillery RW (2002) The role of the thalamus in the flow of information to the cortex. Philosophical Transactions of the Royal Society of London – Series B: Biological Sciences 357: 1695–1708.

78. McCormick DA, Huguenard JR (1992) A model of the electrophysiological properties of thalamocortical relay neurons. Journal of Neurophysiology 68: 1384–1400.

79. Mukherjee P, Kaplan E (1995) Dynamics of neurons in the cat lateral geniculate nucleus: in vivo electrophysiology and computational modeling. Journal of Neurophysiology 74: 1222–1243.

80. Smith GD, Cox CL, Sherman SM, Rinzel J (2000) Fourier analysis of sinusoidally driven thalamocortical relay neurons and a minimal integrate-and fire-or-burst model. Journal of Neurophysiology 83: 588–610.

81. Reinagel P, Godwin D, Sherman SM, Koch C (1999) Encoding of visual information by LGN bursts. Journal of Neurophysiology 81: 2558–2569.

82. Wolfart J, Debay D, Le Masson G, Destexhe A, Bal T (2005) Synaptic background activity controls spike transfer from thalamus to cortex. Nature Neuroscience 8: 1760–1767.

83. Sherman SM (1996) Dual response modes in lateral geniculate neurons: mechanisms and functions. Visual Neuroscience 13: 205–213.

84. Hitschfeld ÉM, Stamper SA, Vonderschen K, Fortune ES, Chacron MJ (2009) Effects of Restraint and Immobilization on Electrosensory Behaviors of Weakly Electric Fish. ILAR Journal 50: 361–372.

85. Bastian J, Chacron MJ, Maler L (2002) Receptive field organization determines pyramidal cell stimulus-encoding capability and spatial stimulus selectivity. Journal of Neuroscience 22: 4577–4590.

86. Chacron MJ (2006) Nonlinear information processing in a model sensory system. Journal of Neurophysiology 95: 2933–2946.

87. Toporikova N, Chacron MJ (2009) Dendritic SK channels gate information processing in vivo by regulating an intrinsic bursting mechanism seen in vitro. Journal of Neurophysiology 102: 2273–2287.

88. McGillivray P, Vonderschen K, Fortune ES, Chacron MJ (2012) Parallel coding of first and second order stimulus attributes by midbrain electrosensory neurons. Journal of Neuroscience 32: 5510–5524.

89. Rose GJ, Fortune ES (1996) New techniques for making whole-cell recordings from CNS neurons in vivo. Neuroscience Research 26: 89–94.

90. Frank K, Becker MC (1964) Microelectrodes for recording and stimulation. Physical Techniques in Biological Research, part A. New York: Academic. 23–84.

91. Chacron MJ, Lindner B, Longtin A (2007) Threshold fatigue and information transfer. Journal of Computational Neuroscience 23: 301–311.

92. Chacron MJ, Longtin A, Maler L (2005) Delayed excitatory and inhibitory feedback shape neural information transmission. Physical Review E 72: 051917.

93. Ramcharitar JU, Tan EW, Fortune ES (2005) Effects of global electrosensory signals on motion processing in the midbrain of Eigenmannia. Journal of Comparative Physiology A-Sensory Neural & Behavioral Physiology 191: 865–872.

94. Vonderschen K, Chacron MJ (2009) Sparse Coding of Natural Communication Signals in Midbrain Neurons. Biomedical Central Neuroscience 10: O3.

95. Bastian J, Nguyenkim J (2001) Dendritic Modulation of Burst-like firing in sensory neurons. Journal of Neurophysiology 85: 10–22.

96. Saunders J, Bastian J (1984) The physiology and morphology of two classes of electrosensory neurons in the weakly electric fish Apteronotus Leptorhynchus. Journal of Comparative Physiology A 154: 199–209.

97. Chacron MJ, Maler L, Bastian J (2005) Feedback and Feedforward Control of Frequency Tuning to Naturalistic Stimuli. Journal of Neuroscience 25: 5521–5532.

98. Krahe R, Bastian J, Chacron MJ (2008) Temporal processing across multiple topographic maps in the electrosensory system. Journal of Neurophysiology 100: 852–867.

99. Carr CE, Maler L (1985) A Golgi study of the cell types of the dorsal torus semicircularis of the electric fish Eigenmannia: functional and morphological diversity in the midbrain. Journal of Comparative Neurology 235: 207–240.

100. Manwani A, Koch C (1999) Detecting and estimating signals in noisy cable structure, I: neuronal noise sources. Neural Computation 11: 1797–1829.

101. Lewis JE, Maler L (2002) Dynamics of electrosensory feedback: short-term plasticity and inhibition in a parallel fiber pathway. Journal of Neurophysiology 88: 1695–1706.

102. Lewis JE, Maler L (2004) Synaptic dynamics on different time scales in a parallel fiber feedback pathway of the weakly electric fish. Journal of Neurophysiology 91: 1064–1070.

103. Lindner B, Gangloff D, Longtin A, Lewis JE (2009) Broadband coding with dynamic synapses. Journal of Neuroscience 29: 2076–2087.

104. Harvey-Girard E, Lewis JE, Maler L (2010) Burst-induced anti-Hebbian depression acts through short-term synaptic dynamics to cancel redundant sensory signals. Journal of Neuroscience 30: 6152–6169.